(2)

Annual Report

Nitride Semiconductors for Ultraviolet Detection

Supported under Grant #N00014-92-J-1720
Innovative Science and Technology Office
of the Strategic Defense Initiative
Office of the Chief of Naval Research
Report for the period March 11, 1992–December 31, 1992

Robert F. Davis, K. Shawn Ailey-Trent, Daniel Kester,
Russell Patterson, Bill Perry, Laura Smith, Cheng Wang,
Warren Weeks and Kimberly Webber
Materials Science and Engineering Department
North Carolina State University
Campus Box 7907
Raleigh, NC 27695-7907

December 1992

REPORT DOCUMENTATION PAGE

Form Approved
OMB No 0704 0188

1. AGENCY USE ONLY (Leave blank)	2. REPORT DATE	3. REPORT TYPE AND DATES COVERED
	December 1992	Annual 3/11/92–12/31/92

4. TITLE AND SUBTITLE

Nitride Semiconductors for Ultraviolet Detection

5. FUNDING NUMBERS

s400018srr01
1114SS
N00179
N66005
4B855

6. AUTHOR(S)

Robert F. Davis

7. PERFORMING ORGANIZATION NAME(S) AND ADDRESS(ES)

North Carolina State University
Hillsborough Street
Raleigh, NC 27695

8. PERFORMING ORGANIZATION REPORT NUMBER

N00014-92-J-1720

9. SPONSORING / MONITORING AGENCY NAME(S) AND ADDRESS(ES)

Sponsoring: ONR, 800 N. Quincy, Arlington, VA 22217
Monitoring: Office of Naval Research Resider, N66005
The Ohio State Univ. Research Center
1314 Kinnear Road
Columbus, OH 43212-1194

10. SPONSORING / MONITORING AGENCY REPORT NUMBER

11. SUPPLEMENTARY NOTES

12a. DISTRIBUTION / AVAILABILITY STATEMENT

Approved for Public Release—Distribution Unlimited

12b. DISTRIBUTION CODE

13. ABSTRACT (Maximum 200 words)

Thin films of GaN and $Al_xGa_{1-x}N$ have been deposited by modified gas source MBE on α(6H)-SiC(0001) and sapphire(0001). The values of x ranged from 0 to 1 in intervals of 0.2, as determined scanning Auger spectrometry. Simple UV photo detectors were produced and tested. The gains in the detectors was 10-20 at a bias voltage of 5 volts. The photocurrents for the solid solution detectors were much larger than for the pure GaN. Intrinsic, Mg p-type and Si n-type doped GaN films have also been achieved during growth. GaN thin films have also been achieved via atomic layer epitaxy on SiC substrates from triethygallium and ammonia. Additional efforts have been channeled to develop luminescence facilities operative in the blue–UV wavelength range, ion implantation and contact studies and reactive ion etching facilities for GaN and AlN studies.

14. SUBJECT TERMS

thin films, GaN, AlGaN solid solutions, gas source MBE, SiC(0001), sapphire(0001), photodetectors, p-type GaN, n-type GaN, ion implantation, reactive ion etching

15. NUMBER OF PAGES

52

16. PRICE CODE

17. SECURITY CLASSIFICATION OF REPORT	18. SECURITY CLASSIFICATION OF THIS PAGE	19. SECURITY CLASSIFICATION OF ABSTRACT	20. LIMITATION OF ABSTRACT
UNCLAS	UNCLAS	UNCLAS	SAR

Table of Contents

I. Introduction

Continued development and commercialization of optoelectronic devices, including light-emitting diodes and semiconductor lasers produced from III-V gallium arsenide-based materials, has also generated interest in the much wider bandgap semiconductor mononitride materials containing aluminum, gallium, and indium. The majority of the studies have been conducted on pure gallium nitride thin films having the wurtzite structure, and this emphasis continues to the present day. Recent research has resulted in the fabrication of p-n junctions in wurtzitic gallium nitride, the deposition of cubic gallium nitride, as well as the fabrication of multilayer heterostructures and the formation of thin film solid solutions. Chemical vapor deposition (CVD) has usually been the technique of choice for thin film fabrication. However, more recently these materials have also been deposited by plasma-assisted CVD and reactive and ionized molecular beam epitaxy.

The program objectives in this reporting period have been (1) the growth of thin films of GaN and $Al_xGa_{1-x}N$ solid solutions, (2) the fabrication of the materials into UV photon detectors and their characterization, (3) the deposition via gas-source MBE of intrinsic n- and p-type doped GaN, (4) deposition of monocrystalline GaN via atomic layer epitaxy, (5) the initial conduct of studies regarding the ion implantation of AlN and GaN and (6) design of facilities for luminescence and reactive ion etching of wide bandgap thin film materials. The procedures, results, discussions of these results and conclusions of these studies are summarized in the following sections with reference to appropriate SDIO/ONR reports for details. Note that each major section is self-contained with its own figures, tables and references.

II. Growth of Thin Films of GaN and $Al_xGa_{1-x}N$ Solid Solutions via MBE for UV Photon Detectors

A. Introduction

Group III-V nitrides are promising candidate materials for optoelectronic devices, such as light emitting diodes and semiconductor lasers having emission wavelengths in the blue and ultraviolet regions of the spectrum [1]. It is believed that, like the highly successful As- and P-based materials, the heterostructures of the III-V nitrides (heterostructure quantum wells or even superlattice quantum wells) will become increasingly important for optoelectronic device applications. The advantages of heterostructures, e.g., i) enhanced carrier mobility & improved device speed, ii) engineered bandgaps to produce lasing at desired wavelengths, and iii) greatly enhanced quantum efficiency (carrier confinement in radiative region and a window to the emitted radiation) will enhance the device performance.

Our research regarding the deposition of AlN/GaN multilayer films has shown that heterostructures having abrupt interfaces, both chemically and structurally, as well as good crystal quality [2] can be achieved using modified gas source MBE. Based on these results, we have initiated efforts to make a variety of different solid solution materials to extend the flexibility for future heterostructural devices designs. In the following sections, the preliminary research results concerned with the deposition of $Al_xGa_{1-x}N$ solid solution films is reported. In addition, the results of preliminary device applications of GaN and $Al_xGa_{1-x}N$ solid solution films in UV photon detectors will be presented.

B. Experimental Procedure

The thin film deposition system employed in this research was a commercial Perkin-Elmer 430 MBE system. This system consisted of three parts: a load lock (base pressure of 5×10^{-8} Torr), a transfer tube (base pressure of 1×10^{-10} Torr), which also was used for degas the substrates, and the growth chamber (base pressure of 5×10^{-11} Torr). Knudson effusion cells with BN crucibles and Ta wire heaters were charged with 7N pure Gallium and 6N pure aluminum, respectively. Ultra-high purity nitrogen, further purified by a chemical purifier, was used as the sources gas. The N_2 was decomposed to more reactive species using an ECR plasma source, designed to fit inside the 2.25 inch diameter tube of the source flange cryoshroud. The details of the system can be found elsewhere [3].

The substrates were (0001) oriented α(6H)-SiC and epitaxial quality sapphire wafers. Prior to loading into the chamber, the α-SiC substrates were cleaned using standard degreasing and RCA cleaning procedures. The sapphire substrates were cleaned using the following procedure: degreasing and DI water rinse, emersion for 10 minutes in a 1:1 hot solution of HPO_3:H_2SO_4, a thorough DI water rinse and a brief dip in a 1:10 solution of 49% HF:H_2O.

All cleaned substrates were subsequently mounted on a 3-inch molybdenum block and loaded into the system. After undergoing a degassing procedure (700°C for 30 minutes), the substrates were transferred into the deposition chamber. Reflection high energy electron diffraction (RHEED) was performed to examine the crystalline quality of the substrates.

C. Results

1. Deposition of $Al_xGa_{1-x}N$ Solid Solutions

The goal in this aspect of the research has been the deposition of films of $Al_xGa_{1-x}N$ solid solutions for x ranging from 1 to 0. Composition ratios of Al-atoms to Ga-atoms in the films were varied through control of the Ga-cell and the Al-cell temperatures, respectively. Typical deposition conditions are listed in Table I. RHEED was performed to examine the crystalline quality of the films; it indicated that all the films for x ranging from 1 to 0 to be monocrystalline. The Al/Ga composition ratios in the alloy films were determined using a JEOL JAMP-30 Scanning Auger Microprobe (SAM). The results indicated that real Al/Ga composition ratios were close to the estimated Al/Ga ratios based on Al/Ga flux ratios. A multilayer film which consisted of seven $Al_xGa_{1-x}N$ sublayers was deposited. Ratios of Al/Ga, x, in each sublayer were 1, 0.7, 0.5, 0.3, 0.2, 0.12 and 0 respectively. The RHEED pattern of the top GaN film indicated film had a good crystalline quality.

Table I. Deposition Conditions for Undoped GaN Films

Nitrogen pressure	2×10^{-4} Torr
Microwave power	50W
Gallium cell temperature	945~990°C
Aluminum cell temperature	1120~1030°C
substrate temperature	650°C

2. Optical Device Application of GaN and $Al_{0.12}Ga_{0.88}N$ Films

We have also characterized the GaN and $Al_xGa_{1-x}N$ solid solution films in terms of their optoelectronic properties. Simple UV light photon detectors have been produced and tested. Single crystal GaN or $Al_{0.12}Ga_{0.88}N$ films having a thickness of ~3000Å were first deposited on α-SiC and sapphire substrates using the deposition conditions discussed above. A 1000Å thick Al layer was then in-situ deposited on top of the films at a temperature of 200°C. The top Al layer was further masked and etched by lithographic techniques to form interdigitated

electrode configuration. This interdigtated electrodes had a 1μm spacing. Figure 1 is a schematic illustration of a devices of this type. Current-voltage (IV) measurements in both dark and illuminated states were performed to characterize these devices. A 500 W high pressure Hg arc-lamp with a collimating lens (Oriel model 6285), was used as the ultra-violet illumination source. Figure 2 shows the results of the IV characterization for three of the photon detectors fabricated in this research.

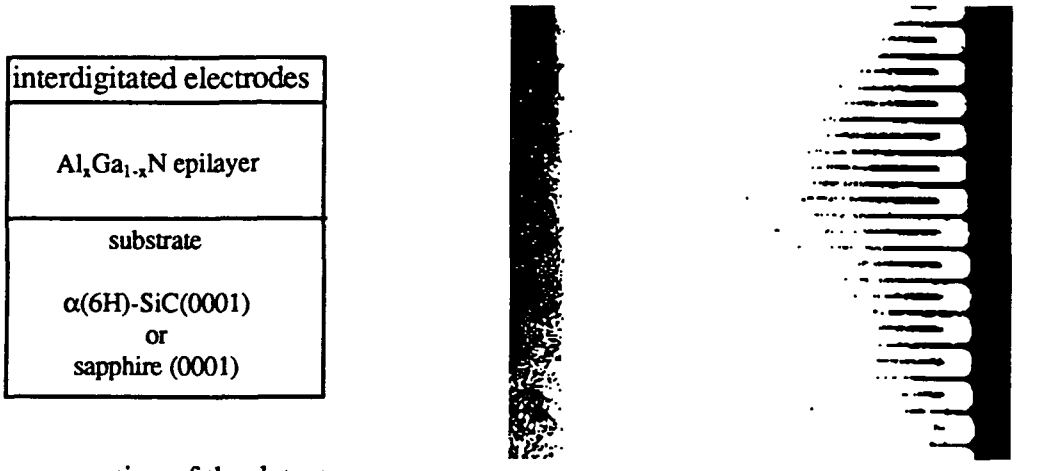

(a) cross-section of the detector

(b) SEM picture of interdigitated electrodes

Figure 1. Schematic illustration of the photoconductive photon detector devices fabricated as described in the text.

These results show that all three detectors exhibited moderately good photoresponse to the UV illumination. The gains of the detectors, defined as

$$G = \text{light current} / \text{dark current}$$

were about same: 10~20 at a bias voltage of 5 volts. The photocurrents for the $Al_{0.12}Ga_{0.88}N$ detectors were much larger than for the GaN detector. At a bias voltage of 5 volts, a photocurrent as large as 10 mA was obtained for the $Al_{0.12}Ga_{0.88}N$ detectors deposited on sapphire substrates.

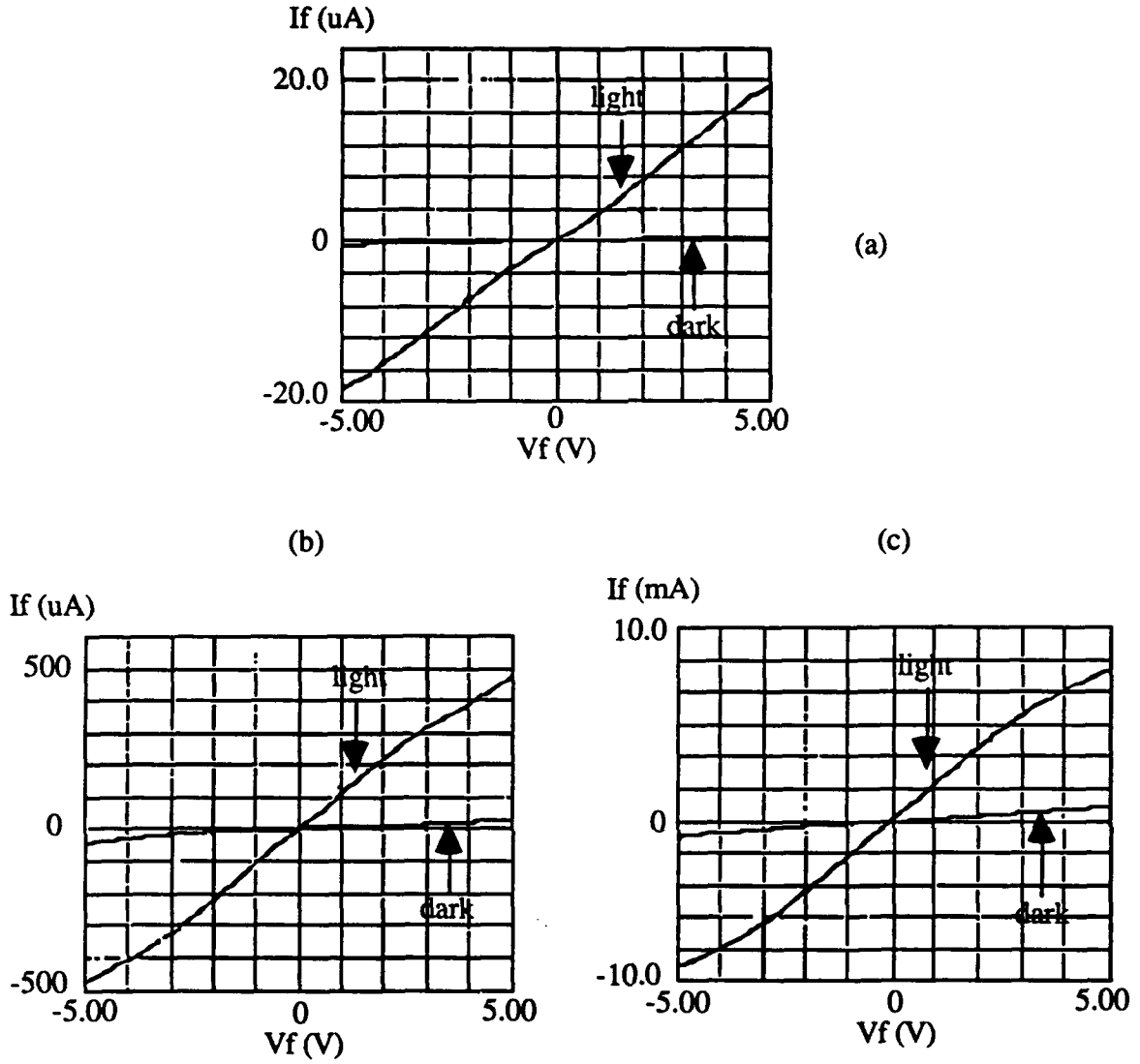

Figure 2. IV measurements for three UV light photon detectors having a photoconductive layer of (a) GaN on sapphire; (b) $Al_{0.12}Ga_{0.88}N$ on sapphire(0001); and (c) $Al_{0.12}Ga_{0.88}N$ on α(6H)-SiC(0001).

Recently, we have found in our research that the crystalline quality of undoped GaN films can be greatly improved by eliminating the amorphous interfacial layer between the substrates and the deposited films. The resulting films exhibited intrinsic electrical behavior. The details of this progress have been reported previously. We have used these improved films for the UV light photon detectors described above. Current-voltage characterization of these devices, under both illuminated and dark environments, indicated that at a bias voltage of 5 volts, the gain increased to as high as ~170. This was primarily due to the large decrease in the dark current. In addition, the photocurrent increased significantly.

D. Summary

Solid solution films of $Al_xGa_{1-x}N$ have been successfully deposited using a modified gas source MBE system. Simple UV detectors made from pure GaN and $Al_xGa_{1-x}N$ solid solutions have been tested. The results showed that III-V nitrides films are excellent candidate materials for UV photon detectors. However, much more research must be conducted to meet the needs of device designers.

E. Future Research Plan

We have shown that $Al_xGa_{1-x}N$ solid solution films can be made in our modified gas source MBE system. These solid solution films were successfully used as the photoconductive material in the photon detectors. To achieve higher gain in the photon detectors, these films must be further optimized. The crystal quality of the films must be improved in concert with their application in photon detector devices. In addition, more device properties, such as response time and spectral response, will be determined.

In a companion section in this report we show that we can produce p-type GaN and p-type $Al_{0.12}Ga_{0.88}N$ films. With this ability, we will concentrate our research efforts on the fabrication of heterostructural device. Also we will continue to study the deposition and characterization of InN films to determine the conditions for achieving $Al_xIn_{1-x}N$ solid solution films in the near future.

F. References

1. R. F. Davis, "Current Status of the Research on III-V Mononitrides Thin Films for Electronic and Optoelectronic Applications," in The *Physics and Chemistry of Carbides, Nitrides and Borides*, R. Freer, ed. Kluwer Academic Publishers, Dordrecht, The Netherlands, 1990, pp.653-669.
2. Z.Sitar, M. J. Paisley, B. Yan, J. Ruan, J. W. Choyke and R. F. Davis, "Growth of AlN/GaN Layered Structures by Gas Source Molecular Beam Epitaxy", J. Vac. Sci. Technol. **B8**, 316 (1990).
3. Z. Sitar, M. J. Paisley, D. K. Smith and R. F. Davis, "Design and Performance of an Electron Cyclotron Resonance Plasma Source for Standard Molecular Beam Epitaxy Equipment," Rev. Sci. Instrum. **61**, 2407 (1990).

III. Deposition via MBE of Intrinsic Undoped, Magnesium Doped p-type and Silicon Doped n-type GaN Films

A. Introduction

During last three decades, the growth and the characterization of GaN films have received considerable attention [1]. However, until recently, the application of this material in terms of devices was relegated to MIS light emitting diodes due to the unsuccessful deposition of p-type films. To date, the introduction during growth of acceptor-like dopants, such as Mg and Zn, resulted only in compensation. For example, the electrical properties of the GaN films changed from being highly conductive n-type, for the undoped film to highly resistive for the acceptor-doped films. However, recently a Japanese research group observed p-type character in a Mg-doped GaN film after a post-deposition Low-Energy Electron-Beam Irradiation (LEEBI) treatment [2]. However, to date there is no explanation for this phenomena. In order to make commercial devices, one should have the capability to activate the acceptor dopants in GaN during the growth and, thus, to make p-type GaN films directly.

In this report, we will show that direct deposition of p-type GaN films has been achieved. We have found that improving the crystalline quality of the deposited GaN film caused its electrical properties to change from a highly n-type material to one having a very high resistance. In our research, this was accomplished by preventing the formation of a thin amorphous interfacial layer on the SiC substrate and by growing a AlN buffer layer on both the SiC and the sapphire substrates. Furthermore, we have shown for the first time that as-deposited p-type GaN films can be produced using this deposition procedure.

The effect of Si doping has also been investigated. Only films deposited on sapphire have been doped due to the limited supply of α-SiC substrates. Preliminary results indicated that n-type GaN films were obtained by Si doping. The resistivity and carrier concentration of these films were $\approx 10^{-2}$ Ω·cm and $\sim 6\times10^{18}$ cm^{-3}, respectively.

B. Experimental Procedure

The deposition system employed in this research was a commercial Perkin-Elmer 430 MBE system. This system consists of three parts: a load lock (base pressure of 5×10^{-8} Torr), a transfer tube (base pressure of 1×10^{-10} Torr), which also was used for degas the substrates, and the growth chamber (base pressure of 5×10^{-11} Torr). Knudson effusion cells with BN crucibles and Ta wire heaters were charged with 7N pure Gallium, 6N pure aluminum, 6N pure magnesium and 6N pure silicon respectively. Ultra-high purity nitrogen, further purified by a chemical purifier, was used as the sources gas. And it was excited by an ECR plasma source, which was designed to fit inside the 2.25 inch diameter tube of the source flange cryoshroud. The details of the system can be found elsewhere [3].

The substrates were (0001) oriented α(6H)-SiC and epitaxial quality sapphire wafers. Prior to loading into the chamber, the α-SiC substrates were cleaned by a standard degreasing and RCA cleaning procedure. The sapphire substrates were cleaned using the following procedure: degreasing and DI water rinse, 10 minutes in a hot solution of HPO_3:H_2SO_4 with 1:1 ratio, DI water rinse, finally dip in 1:10 solution of 49% HF:H_2O. All substrates were mounted on a 3-inch molybdenum block and loaded into the system. After undergoing a degassing procedure (700°C for 30 minutes), the substrates were transferred into the deposition chamber. Finally RHEED was performed to examine the crystalline quality of the surfaces of the substrates.

C. Results

Deposition of high quality undoped GaN films. In the past, single crystal GaN films have been successfully deposited on a variety of substrates using the NCSU modified gas source MBE system. However, the resistivity of those as-deposited films was low, and they exhibited an n-type character. We have also found for the films deposited on α-SiC (0001) substrates, a thin amorphous silicon nitride layer existed at the interface of substrates and the deposited GaN films [4]. This resulted from the interaction of activate nitrogen species produced in the ECR plasma source with the SiC surface prior to opening the Ga or Al shutter at the outset of the deposition. The RHEED pattern of both the α-SiC and sapphire substrates changed after exposure to the nitrogen plasma. We found that this change could occur for exposure to the nitrogen plasma for times as little as five minutes.

We have developed the following technique to prevent this amorphous interfacial layer from forming on the substrate surface. The procedure involves an initial exposure of the substrate to pure Al followed by the exposure of this Al to reactive N. During this time, these Al layers reacted with the plasma activated nitrogen species and formed an AlN layer. The details of re-acting metal Al with activated N_2 species to form AlN can be found in a report by J. A. Taylor [5]. The film growth was subsequently initiated using the deposition conditions listed in the Table I.

Table I. Deposition Conditions for Undoped GaN Films

Nitrogen pressure	2×10^{-4} Torr
Microwave power	50W
Gallium cell temperature	990°C
Aluminum cell temperature	1120°C
substrate temperature	650°C
Al layer	2 monatomic layer
AlN buffer layer	150~200Å
GaN	4000~5000Å

An AlN buffer layer having a thickness of about 150Å was used to reduce the lattice mismatch between the substrate and GaN [6]. Reflection High Energy Electron Diffraction (RHEED) and SEM were performed to examine the quality of the deposited GaN films. RHEED patterns taken on the <2$\bar{1}\bar{1}$0> azimuth of GaN films deposited on (0001)-oriented α-SiC and sapphire substrates are shown in Figure 1. An analysis of these RHEED patterns indicated that both the AlN buffer layer and the GaN film are monocrystalline films. The RHEED pattern of the final surface of the GaN films indicated that they possessed reasonable crystalline quality and a smooth surface. Kikuchi lines were observed on the RHEED screen, but can not be photographed due to the low contrast. A spotty RHEED pattern was obtained for the GaN film deposited on the sapphire substrate due to sample charging of the resistive film. This is also discussed below. The surface morphology of the films was also examined by SEM. The featureless picture, shown in Figure 2, is indicative of the smooth surface of the deposited GaN film and agreed well with the RHEED pattern results.

Deposition of Mg-doped GaN films. Based on above results, we investigated the incorporation of the acceptor dopant, Mg, into the films. The deposition conditions for Mg-doped GaN films were same as that for undoped GaN films described before, except that a Mg-source was used in the deposition. Table II lists the typical deposition conditions for Mg-doped GaN films.

Table II. Deposition Conditions for Mg-doped GaN Films

Nitrogen pressure	2×10^{-4} Torr
Microwave power	50W
Gallium cell temperature	990°C
Aluminum cell temperature	1120°C
Magnesium cell temperature	~300°C
substrate temperature	650°C
Al layer	2 monatomic layer
AlN buffer layer	150~200Å
Mg-doped GaN	4000~5000Å

(a)

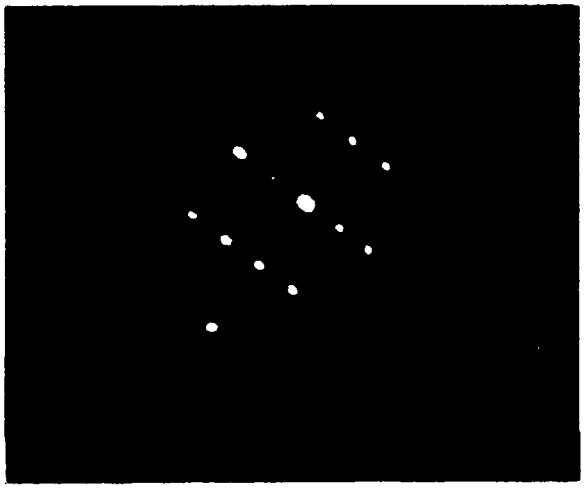

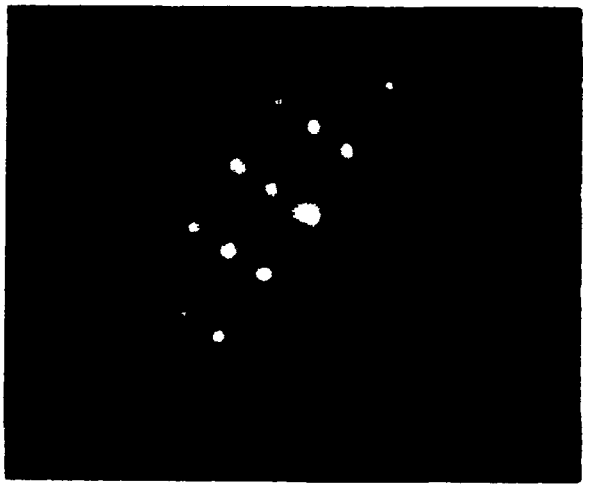

(b) (c)

Figure 1. RHEED patterns taken in the <2ΓΓ0> azimuth of a) AlN buffer layer on α-SiC substrate, b) GaN film on AlN/α-SiC substrate, c) GaN film on AlN/sapphire substrate.

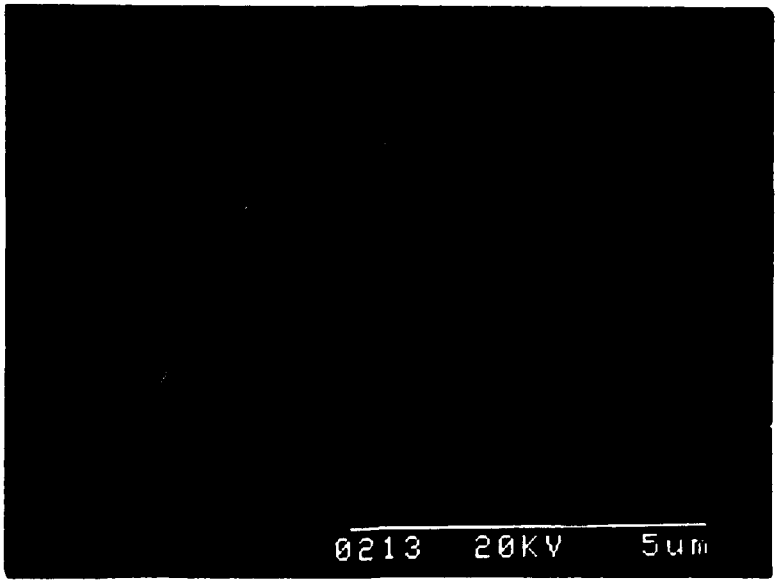

Figure 2. SEM photograph of the surface of an undoped GaN film deposited on a AlN/α-SiC substrate.

The RHEED patterns of the Mg-doped films also showed features indicative of good crystalline quality. The representative SEM picture in Figure 3 shows that the Mg-doped GaN film also had a very smooth surface.

Electrical properties of undoped and Mg-doped GaN films. The electrical properties of the films have been characterized using the van der Pauw resistivity measurement technique and Hall effect measurements. Indium was used as the electrical contacts. Current-voltage (IV) measurements were first performed to check the contact character. As shown in Fig. 4(a), the undoped GaN film was quite resistive; a non-ohmic IV character was observed after a voltage larger than 15 volts was applied. The Mg-doped GaN films was much more conductive, as shown in Fig. 4(b), and IV measurements of the contacts indicated ohmic character. It is clear from this point that eliminating the amorphous interfacial layer at the substrate surface results in a dramatic improvement in the electrical properties. The early work conducted in our research group showed that even Mg-doped GaN made at that time possessed a non-ohmic IV character similar to that of the undoped GaN films made in this reporting period [7]. Resistivity and Hall effect measurements were performed for both undoped and Mg-doped GaN films. The results were summarized in the Table III. Note that for the undoped GaN films, the highly resistive character made the electrical measurements very difficult. By contrast, for the Mg-doped GaN films, a p-type conductive character was identified, and the measured electrical properties were similar to those recently reported for the low-energy electron-beam irradiation (LEEBI) treated Mg-doped GaN film [2,8]. Furthermore, the p-type conductive character of the Mg-doped films were also identified by the thermal-probe method.

Table III. Electrical Properties of Undoped and Mg-doped GaN Films

films	undoped GaN	Mg-doped GaN
resistivity (Ω·cm)	$>10^2$	0.3
conductive type	x	P-type
mobility ($cm^2/V·s$)	?	~10
carrier concentration (cm^{-3})	$<10^{16}$	$\sim 1\times10^{18}$

Figure 3. SEM photograph of the surface of the undoped GaN film deposited on an AlN/α-SiC substrate.

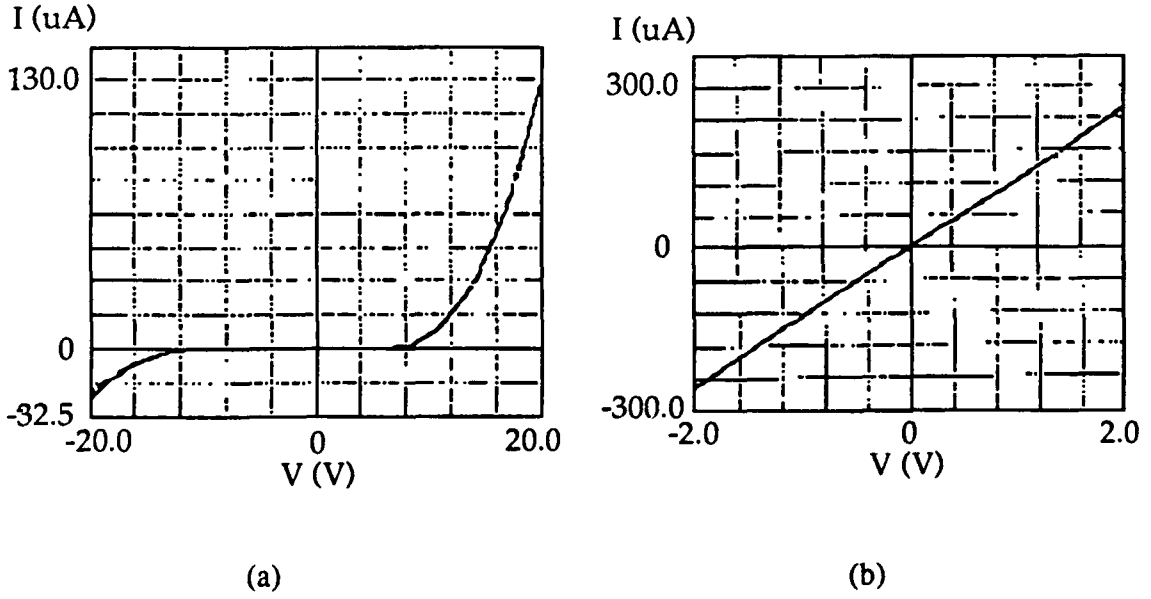

Figure 4. IV Curves for (a) an undoped GaN film, (b) a Mg-doped GaN film.

The temperature dependence of the resistivity for a p-type Mg-doped GaN film has also been measured. The results are shown in Figure 5. The resistivity decreased with increasing temperature due to the increasing ionization of the Mg acceptors.

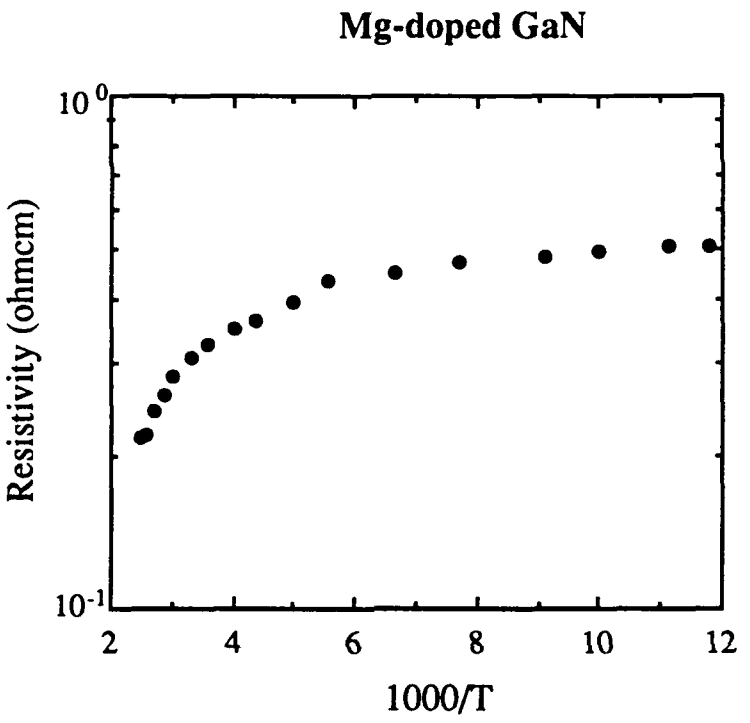

Figure 5. Temperature dependence of resistivity for a Mg-doped p-type GaN film.

Growth of Si-doped GaN films on (0001) sapphire substrates. Based on the results that undoped GaN films were highly resistive, we have investigated the incorporation of the donor-like dopant, Si, into the films to obtain n-type GaN films. The Si-doping process was accomplished in the same manner as the Mg-doping described above. The deposition conditions for producing Si-doped GaN films were the same as that for undoped GaN films, but with the use of the Si-source. This study has been conducted only on the films deposited on (0001) sapphire substrates due to the limited supply of α-SiC substrates. Table IV lists the typical deposition conditions employed to produce these films.

The Si-concentration in the films was varied by controlling the Si-cell temperature. RHEED patterns of the Si-doped films indicated that the film structure changed with an increase in the temperature of the Si-cell. Polycrystalline RHEED patterns occurred for the films deposited with Si-cell temperatures exceeding 1180°C.

Table IV. Deposition Conditions for Si-doped GaN Films

Nitrogen pressure	2×10^{-4} Torr
Microwave power	50W
Gallium cell temperature	990°C
Aluminum cell temperature	1120°C
Silicon cell temperature	900~1300°C
substrate temperature	650°C
Al layer	2 monatomic layers
AlN buffer layer	150~200Å
Si-doped GaN	4000~5000Å

The effect of Si doping on the electrical properties of GaN films was again investigated using the van der Pauw resistivity measurement and Hall effect measurements. It was found that GaN films deposited with the Si-cell temperature lower than 1180°C, were still very resistive. When the Si-cell temperatures reached 1200°C or higher, doped GaN films became very conductive, with a resistivity of $10^{-1}\Omega\cdot$cm or less. However, each of these films showed a polycrystalline RHEED pattern. The maximum Si-cell temperature at which doped GaN films still showed a single crystal RHEED pattern was 1180°C.

The atomic Si-concentration in the films was characterized by SIMS measurements and compared to the free carrier concentration determined by Hall effect measurements. It was found that generally in these Si-doped GaN films, as shown in Figure 6. The atomic Si composition was about two orders higher than the free carrier concentration. This large concentration of inactive Si atoms leads to the degradation of the crystal quality of the film resulting finally in the formation of polycrystalline material. We subsequently limited the temperature of the Si-cell to 1180°C. The typical electrical properties of the Si-doped GaN films are listed in the Table V.

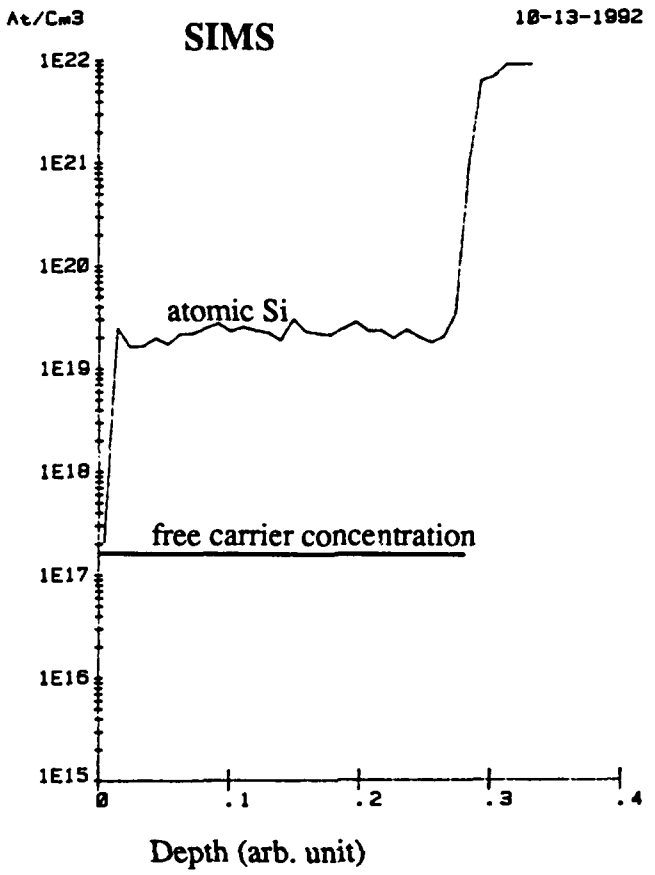

Figure 6. SIMS profile for the Si doped GaN film deposited at the Si-cell temperature of 1180°C.

Table V. Electrical Properties of Undoped and Si-doped GaN Films

	Si-doped GaN
Si-cell temperature	1180°C
conductive type	N
resistivity (Ω·Πcm)	31
carrier concentration (cm^{-3})	1.7×10^{17}
atomic Si concentration (cm^{-3})	2×10^{19}

As indicated above, a certain concentration of the atomic Si in the films was electrically inactive. To further activate these atomic Si, the deposition temperature was increased. The results shown in Table VI indicate that with increasing deposition temperature to 950°C, the

deposited films became more conductive. The resistivity decreased to 0.02Ω·cm, and the free carrier concentrations increased to $5.6\times10^{18}cm^{-3}$. However with a further increase in deposition temperature above 1050°C, the films again became resistive. RHEED measurements indicated that the films deposited at temperature of 1000°C or higher had very rough surfaces. Another problem also occurred at high deposition temperature, namely, the sample surfaces were contaminated by the silver paste mounting material.

Table VI. Effect of Deposition Temperature on Electrical Properties of Si-doped GaN Films

deposition temperature	resistivity (Ω·cm)	carrier concentration (cm^{-3})
650	10.6	1.7×10^{17}
850	0.14	4.3×10^{18}
950	0.02	5.6×10^{18}
1050	too resistive	?

We have also investigated another way to activate the excess atomic Si. In this approach the growth surface was exposed to a UV lamp during deposition, while keeping the substrate temperature at 650°C. The lamp was a 500W mercury arc lamp that was installed in front of a sapphire view port in the center of the source flange and oriented normal to the substrate. The illumination intensity at the growth surface was estimated at about 0.4 W/cm^2 [8]. Preliminary studies have shown that under the same deposition conditions, the resistivities decreased from 10.6 Ω·cm for a film deposited without the lamp illumination to about 0.03 Ω·cm for a film deposited with the lamp illumination; the free carrier concentration increased from 1.7×10^{17} cm^{-3} to about 3.7×10^{18} cm^{-3}.

Electron Microscopy Characterization of Films. The microstructures of the films discussed in this report were further characterized by scanning electron microscopy (SEM) and transmission electron microscopy (TEM). SEM was performed in a Hitachi S-800 SEM with a field emission gun. The samples were coated with a thin conductive layer of carbon to avoid charging effects. Carbon was deposited on a different area of the sample than that used for preparation of TEM samples. Unless otherwise noted, TEM was performed in a JEOL 4000EX operated at 400kV. High Resolution images were recorded using a 1mr convergence semi-angle at Scherzer defocus (~ -47nm). Cross-sectional transmission electron microscopy (XTEM) samples were prepared using standard techniques.

As described earlier, high quality undoped GaN films have been achieved by eliminating the interfacial amorphous layer. The small dimensional features in the surface morphology in the SEM image of the film deposited with the AlN buffer layer, shown in Figure 7, indicated a smooth surface of the deposited GaN film and agreed well with the RHEED pattern results. However, high resolution TEM results revealed the films, deposited on both α-SiC and sapphire substrates, had a columnar structure, as shown in Figure 8, although the RHEED patterns indicated single crystal material. This contradiction is due to the very high degree of preferred orientation of the columns. The defects creating the columnar structure appear to originate at the AlN/SiC interface; however, they increase in number at the GaN/AlN interface. TEM also revealed a rough interface between the AlN and GaN layers, as shown in Figure 8.

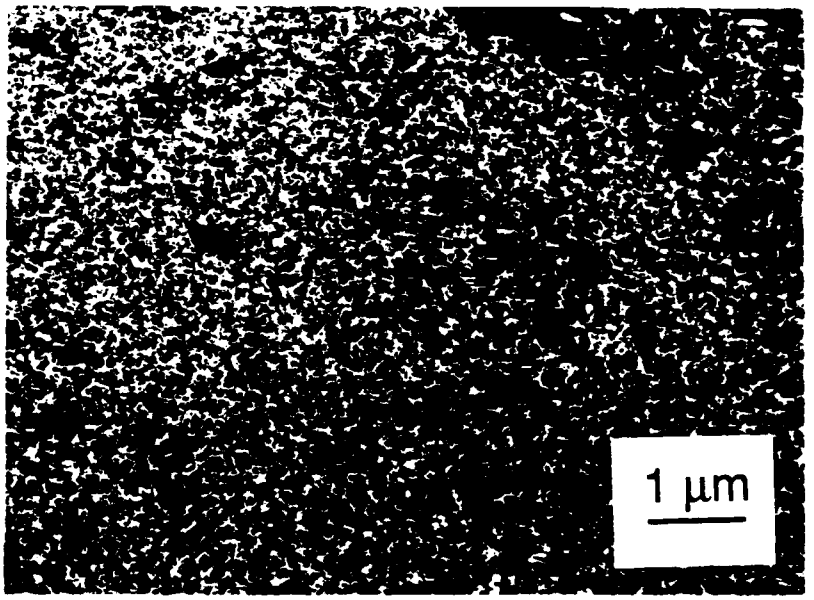

Figure 7. SEM micrograph of the undoped GaN film.

The growth of high quality, single crystal films of AlN has been achieved on α-SiC substrates at higher deposition temperatures (~1100°C) in other research in our group [9]. Therefore, in an attempt to eliminate the columnar structure, we have deposited the thin AlN buffer layer at a higher temperature (1100°C), followed by the deposition of GaN at 650°C. The SEM analysis showed very small surface features; although, XTEM revealed that the film again consisted of a columnar structure. No apparent improvement was gained from the increase in deposition temperature of the buffer layer.

Because there was an increase in the number of defects at the GaN/AlN interface, the effects of the deposition of GaN films on α-SiC substrates without the aide of a buffer layer was investigated at 650° C. A columnar morphology was also observed. It was initiated at the

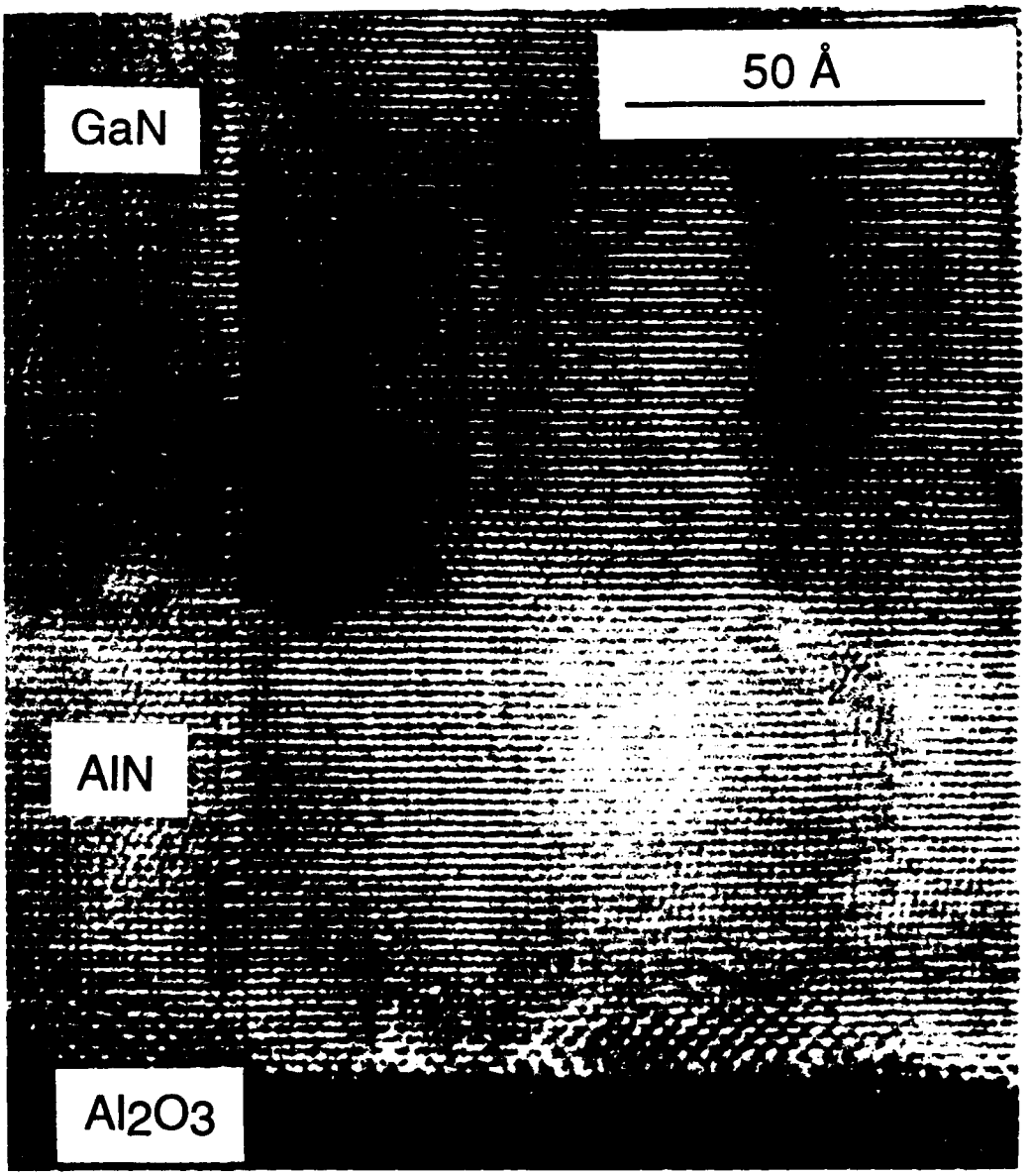

Figure 8(a). TEM micrograph of the undoped GaN films on (a) sapphire (microscopy performed on a Topcon 002B).

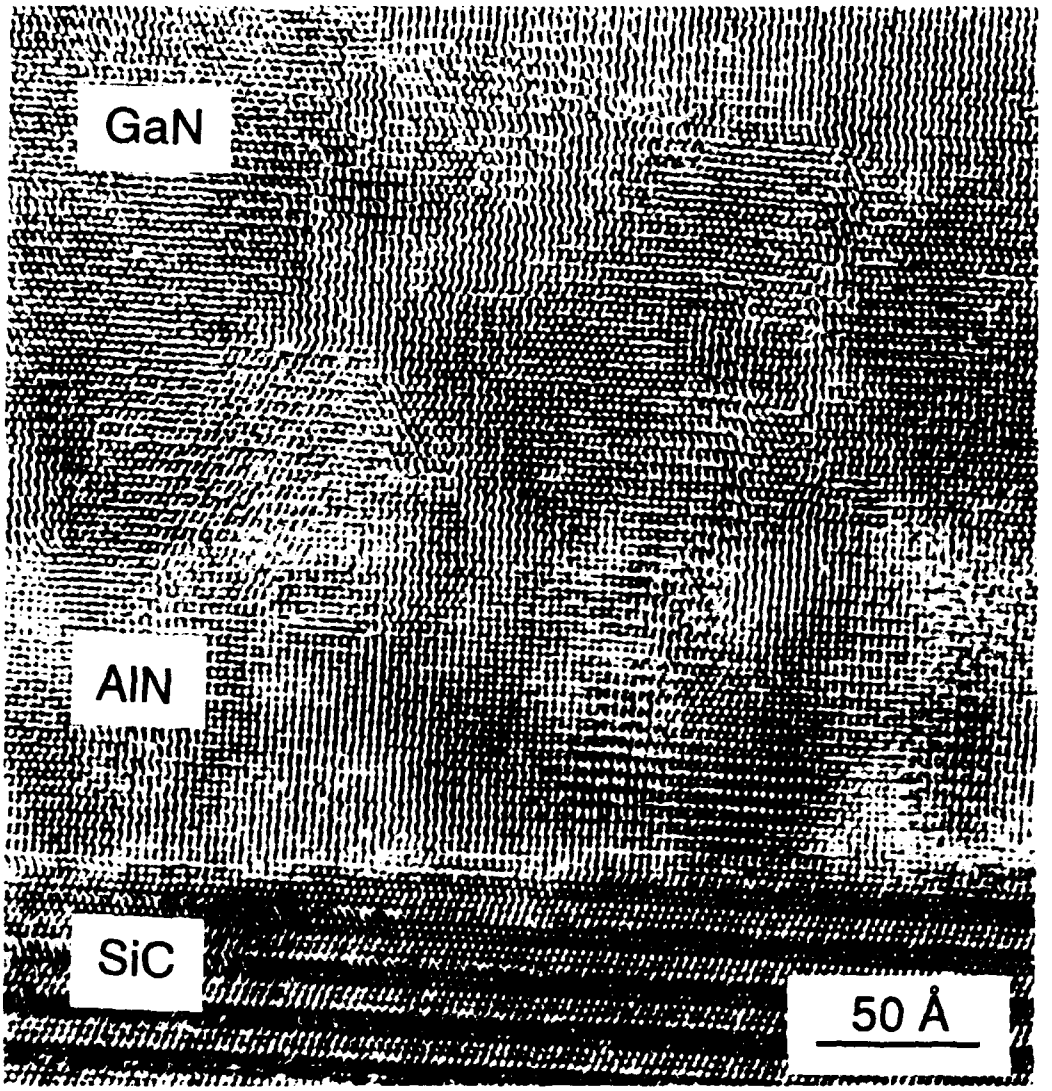

Figure 8(b). TEM micrograph of the undoped GaN films on (b) α-SiC substrates.

SiC/GaN interface. The cause of the columnar structure is possibly the lattice mismatch between the GaN and the α-SiC substrate.

Though AlN has been used as a buffer layer between GaN and the substrates by most research groups, there is still a 2.4% lattice mismatch at the GaN/AlN interface, which could cause the formation of the columnar structure. To avoid this lattice mismatch, we attempted the deposition of a compositionally graded buffer layer subsequent to the growth of the pure AlN film. The goal was to continuously change the composition of this layer from pure AlN to pure GaN. This layer was followed by the deposition of a GaN film. The SEM micrograph of this film, shown in Figure 9, reveals a rough surface which is indicative of a polycrystalline material. XTEM analysis confirmed the polycrystalline nature of the film, as shown in Figure 10. Selected area diffraction (SAD) reveals that the GaN is first deposited in the wurtzite structure but converts to a cubic structure as deposition is continued. This is very likely due to the action of the numerous stacking faults. This micrograph also shows that there was an abrupt change from the AlN to the GaN instead of a gradually graded layer. This is very likely caused by the much stronger attraction of Al to N than the attraction of Ga to N. Further research will attempt to improve the deposition of the graded layer.

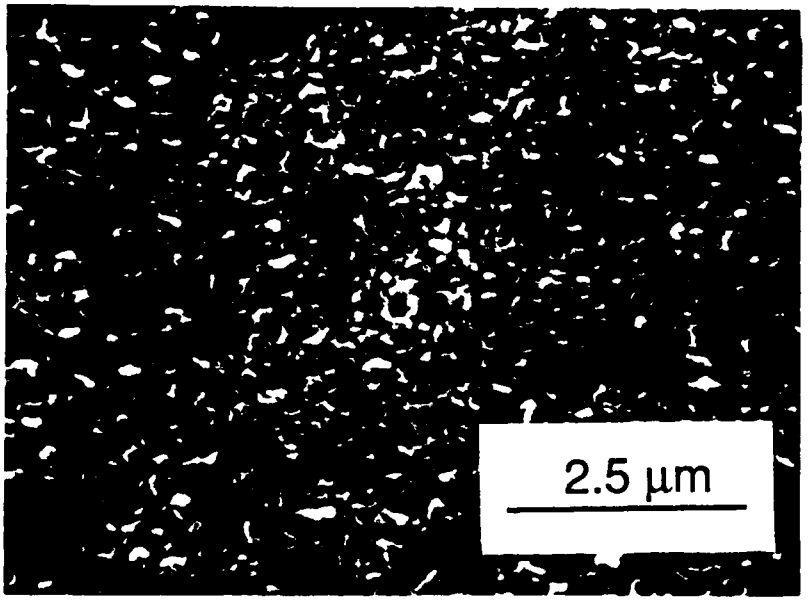

Figure 9. SEM image of an undoped GaN film deposited with a graded $Al_xGa_{1-x}N$ layer.

By comparison to chemical vapor deposition (CVD) in which the growth temperature for GaN films is as high as 1200°C, our modified gas source MBE technique employs a much lower deposition temperature (650°C). Subsequent growth examined the effects of depositing both the buffer layer and the GaN film at higher temperatures (1100°C). XTEM analysis

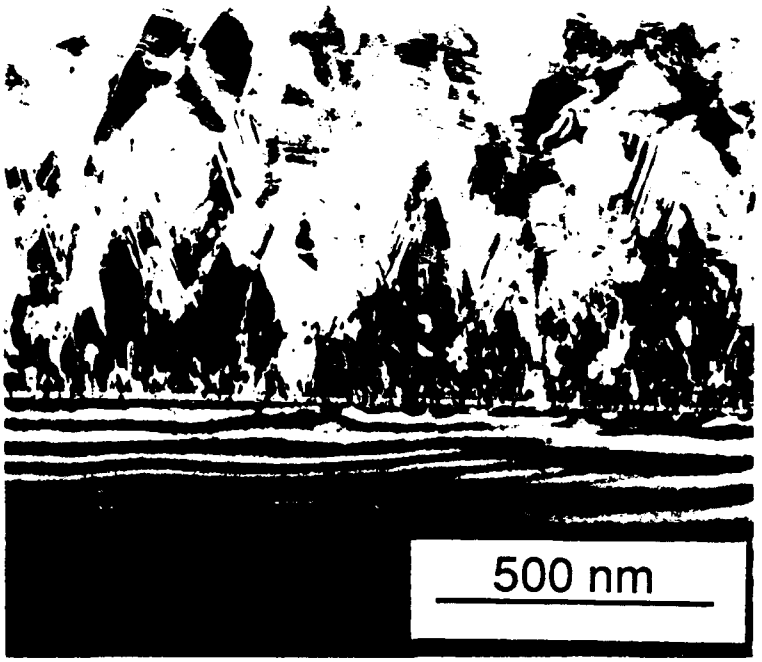

Figure 10. TEM micrograph of an undoped GaN film with a graded $Al_xGa_{1-x}N$ layer.

revealed that the GaN portion of the film was no longer continuous. From these preliminary results, it is tentatively believed that the plasma may be etching the growth surface as the film is being deposited, particularly at these high temperatures. This would create a rough surface in which defects easily form and a columnar structure results. Further investigation is needed to study the effects of ECR plasma source on the structure of deposited films. It may also be that at the much lower beam pressures used in MBE (10^{-4}–10^{-5} Torr) relative to CVD (1 atm), the GaN is unstable to thermal evaporation.

D. Discussion

Undoped GaN films, made by different groups or by different deposition techniques, have been almost universally reported to be conductive and to exhibit n-type conductive character. By contrast, as-deposited Mg-doped GaN films resulted only in being compensated and were very resistive. No as-deposited p-type GaN films had been reported, though a Japanese research group had reported that p-type conductive character is observed on Mg-doped GaN films exposed to post-deposition low-energy electron-beam irradiation [2]. Thus, the question is raised as to why p-type GaN films can not be deposited directly. Moreover, what prohibits the activation of an acceptor dopant? Finally, is the LEEBI treatment the only way to produce p-type GaN films and, if so, why? Answers for these are far from clear yet at this time.

Recently S. Nakamura et. al. postulated from experimental evidence that the acceptor (e.g. Mg)-H neutral complexes formed in as-deposited Mg-doped GaN films and were responsible

for the unsuccessful p-type doping. In addition, these complexes were decomposed by a low-energy electron-beam irradiation treatment. This resulted in the activation of the acceptor dopant and the achievement of p-type doping [10]. However, as yet they have provided no chemical evidence for the existence of hydrogen in their GaN films. We believe that the deactivation of the acceptor dopants in the GaN films may also be related to the existence of a large density of defects, which could trap these dopants. Some of the dopant atoms may be weakly bonded to these defects. The LEEBI treatment, breaks these weak bonds and results in the activation of the acceptor dopants.

Our research group has shown previously [7] that, even under the best deposition conditions, undoped GaN films were still conductive and n-type while Mg-doped GaN films were very resistive. Some changes were also observed after our LEEBI treatment, but they were not as dramatic as the Japanese have reported. In contrast to these early research results, our recent work has shown that by eliminating the amorphous interfacial layer between the substrates and the deposited films, the crystalline quality of the deposited GaN film can be greatly improved. In this way, deposited undoped GaN films become intrinsic, while Mg-doped GaN films become p-type films. This is the further evidence that unsuccessful p-type doping in prior research in other laboratories was mainly due to the existence of electrically activated micro-structural defects in the deposited films.

It also should be pointed out that although as-deposited p-type GaN films can be produced, the hole mobility is quite low. Thus, is low hole mobility an intrinsic property of GaN films or is it caused by their poor microstructural quality? It is well known that the lack of lattice matched substrate materials for GaN make heteroepitaxy quite difficult. A large amount of lattice mismatch still exists even when AlN is used as a buffer layer. We believe that micro-structural defects related to the lattice mismatch can be further reduced if we can find the "right" substrates, such as using a graded $Al_xGa_{1-x}N$ solid solution as a buffer layer. Furthermore, from our high resolution TEM work presented in this report, we have found that the undoped GaN films possess the columnar structure, and the columnar structure definitely contains a high density of defects which may be the cause of the low carrier mobility. No other researchers have presented TEM data that is necessary to determine the effects of columnar structure on possible device fabrication.

E. Conclusions

We have shown that in the use of our modified gas source MBE system, a thin amorphous layer was formed on the surfaces of the SiC and sapphire substrates during exposure to the nitrogen plasma prior to the deposition of the AlN or GaN films. This was prevented by exposing the substrate to an Al or Ga flux sufficient to deposit a submonolayer of metal prior to starting the nitrogen plasma. As a result, the undoped GaN films showed intrinsic electrical

character and were very resistive. Furthermore, by in-situ incorporation of Mg into the films, as-deposited, p-type GaN films were produced for the first time. These latter films had a resistivity = 0.5 Ω·cm, a Hall mobility = 10 $cm^2/V \cdot s$ and a carrier concentration of 1×10^{18} cm^{-3}, respectively. Si-doped n-type GaN films have also been achieved.

F. Future Research Plans

As noted in the Discussion Section of this report, a graded $Al_xGa_{1-x}N$ solid solution may also be chosen as the buffer layer for the homoepitaxy of GaN. Therefore, some of our future efforts will involve the growth of a good quality graded $Al_xGa_{1-x}N$ solid solution buffer layer. The purpose of this study will be to improve the microstructure and carrier mobility of the deposited GaN. The growth of n- and p-type GaN films will be further investigated. Also the cause of the columnar structure in the films will be further investigated and eliminated.

G. References

1. R. F. Davis, "Current Status of the Research on III-V Mononitrides Thin Films for Electronic and Optoelectronic Applications," in The *Physics and Chemistry of Carbides, Nitrides and Borides*, R. Freer, ed. Kluwer Academic Publishers, Dordrecht, The Netherlands, 1990, pp. 653-669.
2. H. Amano, M. Kito, K. Hiramatsu and I. Akasaki, Jap. J. Appl. Phys. **28**, l2112 (1989).
3. Z. Sitar, M. J. Paisley, D. K. Smith and R. F. Davis, "Design and Performance of an Electron Cyclotron Resonance Plasma Source for Standard Molecular Beam Epitaxy Equipment," Rev. Sci. Instrum. **61**, 2407 (1990).
4. Z. Sitar, L. L. Smith and R. F. Davis, "Morphology and Interface Chemistry of the Initial Growth of GaN and AlN on a-SiC and Sapphire," MRS Symp. Proc. **237**, 583 (1991).
5. J. A. Taylor and J. W. Rabalais, "Reaction of $N2^+$ beam with Aluminum Surfaces," J. Chem. Phys. **75**, 1375 (1981).
6. S. Yoshida, S. Misawa and S. Gonda, "Improvements on the Electrical and Luminescent Properties of Reactive Molecular Beam Epitaxy Grown GaN Films by Using AlN-coated Sapphire Substrates," Appl. Phys. Lett. **42**, 427 (1983).
7. R. F. Davis et. al., "The Effect of Electron Beam Irradiation on Mg Doped GaN Thin Films" in Final Technique Report N00014-86-K-0686 P5, 35 (1992).
8. M. Paisley, Ph.D. Thesis, 1992, NCSU, Raleigh
9. L. Rowland, Ph.D. Thesis, 1992, NCSU, Raleigh.
10. S. Nakamura, N. Iwas, M. Senoh and T. Mukai, "Hole Compensation Mechanism of p-type GaN Films," Jpn. J. Appl. Phys. **31**, 107 (1992).

IV. Deposition of GaN by Atomic Layer Epitaxy

A. Introduction

Atomic layer epitaxy (ALE) is the sequential chemisorption of one or more elemental species or complexes within a time period or chemical environment in which only one monolayer of each species is chemisorbed on the surface of the growing film in each period of the sequence. The excess of a given reactant which is in the gas phase or only physisorbed is purged from the substrate surface region before this surface is exposed to a subsequent reaction. This latter reactant chemisorbs and undergoes reaction with the first reactant on the substrate surface resulting in the formation of a solid film. There are essentially two types of ALE which, for convenience, shall be called Type I and Type II.

In its early development in Finland, the Type I growth scenario frequently involved the deposition of more than one monolayer of a given species. However, at that time, ALE was consided possible only in those materials wherein the bond energies between like metal species and like nonmetal species were each less than that of the metal-nonmetal combination. Thus, even if multiple monolayers of a given element were produced, the material in excess of one monolayer could be sublimed by increasing the temperature and/or waiting for a sufficient period of time under vacuum. Under these chemical constraints, materials such as GaAs were initially thought to be improbable since the Ga-Ga bond strength exceeds that of the GaAs bond strength. However, the self-limiting layer-by-layer deposition of this material proved to be an early example of Type II ALE wherein the trimethylgallium (TMG) chemisorbed to the growing surface and effectively prevented additional adsorption of the incoming metalorganic molecules. The introduction of As, however caused an exchange with the chemisorbed TMG such that a gaseous side product was removed from the growing surface. Two alternating molecular species are also frequently used such that chemisorption of each species occurs sequentially and is accompanied by extraction, adstraction and exchange reactions to produce self-limiting layer-by-layer growth of an element , solid solution or a compound.

The Type II approach has been used primarily for growth of II-VI compounds [1-13]; however, recent studies have shown that it is also applicable for oxides [14-18], nitrides [19], III-V GaAs-based semiconductors [20-33] and silicon [34-36]. The advantages of ALE include monolayer deposition control, growth of abrupt p-n junction interfaces, growth of uniform and graded solid solutions with controlled compositions, reduction in macroscopic defects and uniform coverage over large areas. A commercial application which makes use of the last attribute is large area electroluminescent displays produced from II-VI materials. Two comprehensive reviews [37,6], one limited overview [38] and a book [39] devoted entirely to the subject of ALE have recently been published.

The potential semiconductor and optoelectronic applications of III-V nitrides has prompted significant research in thin film growth and development. The materials of concern in this section are GaN, currently, and other III-V nitrides, for future studies. Because GaN in the wurtzite structure with a bandgap of 3.4 eV [40] forms continuous solid solutions with both AlN and InN, for example, which have bandgaps of 6.2 eV [41] and 1.9 eV [42], respectively, engineered bandgap materials could result in optoelectronic devices active from the visible to deep UV frequencies [43].

To produce the desired nitride films, the ALE deposition technique has been implemented. The equipment and procedures used in the current ALE deposition of GaN will be discussed here. The results to date, conclusions and plans for future work are also included.

B. Experimental Procedure

Substrate Cleaning. The appropriate substrate cleaning technique is obviously dependent on the type of substrate being used for ALE deposition. Table I lists some substrate types and their compatible cleaning requirements used during this research. The exact crystal orientation of the substrates used can be found in Table II.

Table I. Substrate Cleaning Techniques

Substrate	Cleaning Technique
Si wafer	Modified RCA procedure
Oxidized SiC wafer	20% HF (10min), then 10% HF (5min)
Other SiC wafer	Modified RCA procedure

Modified RCA procedure: 10min @ 70°C NH_4OH: H_2O_2: DI H_2O (1:1:5 ratios); then DI H_2O rinse; then 10min @ 70°C HCl: H_2O_2: DI H_2O (1:1:5 ratios); then DI H_2O rinse; then 5min 10%HF

Deposition Procedure. Initially, the substrate is loaded onto the SiC-coated, graphite susceptor with variable speed adjustment. The susceptor should be raised to its deposition height in the reactor chamber, approximately one inch below the gas inlet lines. High vacuum conditions of ~ 5×10^{-6} Torr are reached in the chamber before starting depostion.

The ALE reactor design utilizes a continuously rotating susceptor arrangement (Figure 1). Thus, from the diagram, as the susceptor rotates, the substrate is alternately exposed to the metalorganic (MO) gas, the H_2 curtain gas, and the nitrogen source gas (ammonia - NH_3) in a constant cycle. The preference of an organometallic Ga source over a chloride source resulted from higher purity material being available and the fact that transport of the Ga species is easier with metalorganics [43]. For the GaN growth, triethylgallium (TEG) was chosen over trimethylgallium (TMG) because of its lower decomposition temperature range [44].

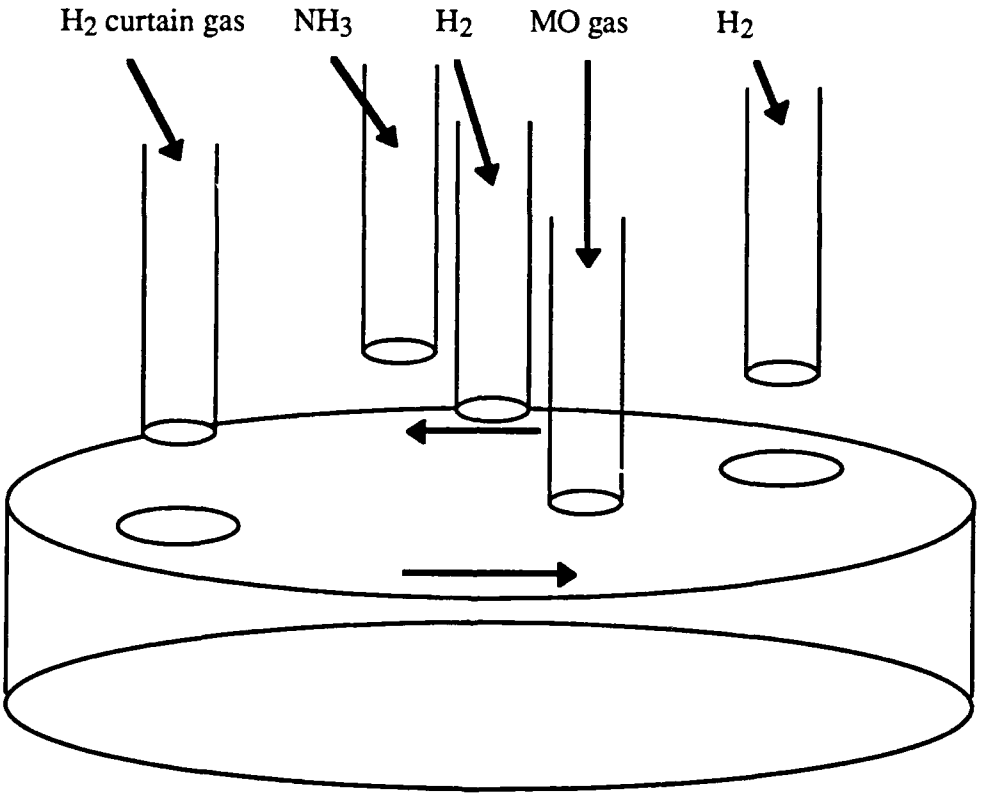

Figure 1. Susceptor design.

Mass Flow Meters and compatible Mass Flow Controllers are utilized to regulate the flow of all gases into the reactor chamber. Once these devices are flowing the setpoint levels of gases and the RF induction heating coils have stabilized the susceptor at the prescribed deposition temperature, rotation of the susceptor can begin. This rotation should begin from under the H_2 inlet line before the MO inlet line. Before the substrate sweeps under the H_2 line after the MO line, the W-filament used in cracking the ammonia into elemental hydrogen and nitrogen should be stabilized at the desired "cracking" temperature.

Once rotation and thus deposition begins, several system variables must be monitored. They include cooling water flow, all gas flow rates, system and MO bubbler pressures,

susceptor and W-filament temperatures, and rotation. Under normal operating procedures, these variables remain nearly constant, but because of their obvious importance, they must be monitored to maintain deposition uniformity. Table II below lists the various system variables for each ALE run attempted.

Table II. Deposition Variables

System Variables	Run # #1	#2	#3	#4	#5
Substrate	Si *	Si *	Si *	SiC **	SiC **
Initial Press.	1×10^{-5} Torr	1×10^{-5}	6×10^{-6}	6×10^{-6}	5×10^{-6}
Run Pressure	3.8-4.1 Torr	3.8-3.9	4.0-4.3	4.1-4.3	4.0-4.3
Bubbler Temp.	74.0°F	69.6	69.6	69.6	61.0
Bubbler Press.	~ 530 Torr	~ 750	~ 750	~ 750	~750
TEG Part. Press.***	5.36 Torr	4.65	4.65	4.65	3.49
H_2 flow	~ 325 sccm	~ 325	~ 325	~ 325	~ 325
NH_3 flow	100 sccm	100	100	100	100
H_2 carrier gas flow	30 sccm	28	28	28	28
TEG flow ***	0.306 sccm	0.175	0.175	0.175	0.131
W-filament Temp.	1410°C	1420	1460	1475	1475
Susceptor Temp.	658°C	636	637	637	637
rpm's	0.4 rpm	0.44	1.0	1.0	1.0
Run Time	90 minutes	130	180	150	150

* Si (100) 3° off-axis toward [011]

** α(6H)-SiC (0001) 3° off-axis toward [$11\bar{2}0$]

*** See equations below for calculation of these values

C. Results

Initially, in Run #1 only a predominantly gallium metal film was deposited with a visibly rough surface texture. For Run #2, the parameters were adjusted (see Table II) to reduce the flow of TEG into the reactor chamber. The resulting film when analyzed using reflected high energy electron diffraction (RHEED) appeared to be highly non-oriented polycrystalline GaN with , once again, a rough surface area. In Run #3 the rotation speed was increased to reduce the exposure time of the substrate to the gallium source gas. Visible surface roughness decreased only slightly. Also, RHEED only revealed ring patterns but no spots, indicating growth of polycrystalline material. For Run #4, a SiC substrate was used keeping all other variables constant. Using RHEED, spot patterns (an indication of a monocrystalline structure) resulted, but no Kikuchi lines were present. In Run #5 a SiC substrate was used, but the partial pressure of TEG in the bubbler was reduced by 25% to lessen the amount of TEG entering the reactor from 0.175 sccm to 0.131 sccm. The deposited film, using RHEED, showed sharp diffraction spots but still no Kikuchi lines (Figure 2). But ultimately, layer-by-layer deposition of monocrystalline GaN on SiC has been achieved.

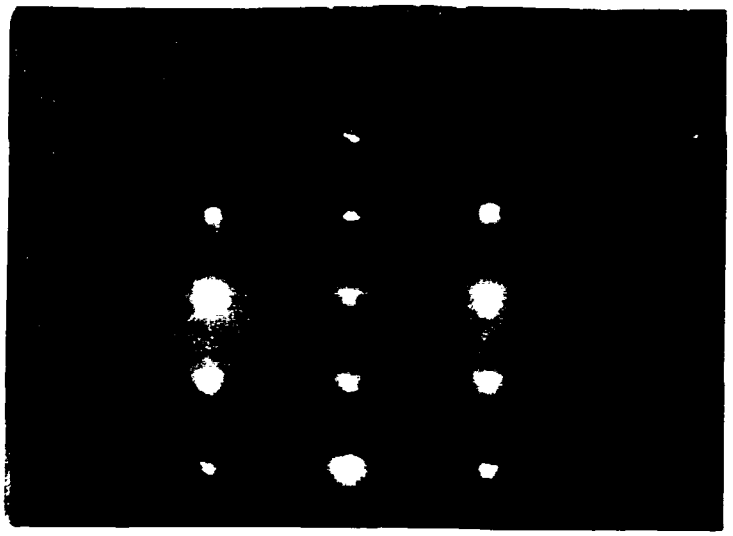

$(2\bar{1}\bar{1}0)$ Reflection

Figure 2. RHEED pattern for GaN deposited on α(6H)-SiC at 637°C.

D. Discussion

The gallium metal deposited during Run #1 was the resultant of excessive TEG entering the reactor. Note from Table II the higher bubbler temperature, higher TEG partial pressure and lower total bubbler pressure yielding this result. TEG levels were subsequently reduced in Run #2 by decreasing the bubbler temperature (i.e. reducing TEG partial pressure) and increasing bubbler pressure. The following equations were used to predict the partial pressure of TEG and its actual flow rate into the reactor chamber.

$$\log P(TEG) = 8.224 - 2222/T(Bubbler)$$

$$F(TEG) = \{F(H_2) \times P(TEG)\}/\{P(Bubbler)-P(TEG)\}$$

where: P(TEG) = partial pressure of TEG in Torr

T(Bubbler) = Bubbler temperature in Kelvin

F(TEG) = TEG flow rate in sccm

$F(H_2)$ = H_2 carrier gas flow rate in sccm

P(Bubbler) = Bubbler pressure in Torr

TEG concentrations were further reduced in Run #3 by increasing the rotation speed. It was concluded that reducing the TEG levels aided in producing polycrystalline GaN, but a rough surface texture continued. The lattice and coefficient of thermal expansion mismatches between the substrate, Si (100), and the GaN film contributed to the polycrystalline growth in Runs #2 and #3. These differences are shown in Table III. For Runs #4 and #5 the substrate used was SiC. The more compatible lattice and coefficient of thermal expansion values aided in the monocrystalline growth of GaN as revealed by RHEED. However, it is apparent that the Ga is not being deposited in a self-limiting manner, but rather by a layer-by-layer mechanism. It is believed that the rough surface on the deposited films may be "pools" of excess Ga or small island nucleations of GaN on the surface. Scanning electron microscopy (SEM) will be utilizes to determine the exact nature of the surface roughness. Slightly excessive concentrations of Ga are still thought to be entering the reactor.

Table III. Physical properties of GaN and potential substrate material [45]

Material	Lattice parameter a (Å)	Lattice parameter c (Å)	Coefficient of thermal expansion (K^{-1})
GaN	3.189	5.185	5.59×10^{-6}
			3.17×10^{-6}
Si	5.43		3.59×10^{-6}
α(6H)-SiC	3.08	15.12	4.2×10^{-6}
			4.7×10^{-6}

E. Conclusions

The effects of reducing the concentration of TEG entering the reactor chamber reveal that deposition does not occur in a self-limiting manner, but rather in a layer-by-layer mechanism.

Thus, it is believed that layer-by-layer deposition resulting in monocrystalline GaN has been achieved using the described deposition procedure. Further analysis will determine the quality of the films deposited.

F. Future Research Plans/Goals

Existing films will be further analyzed to determine the nature of the surface roughness. Also, determination of the defect density using Transmission electron microscopy (TEM) has not yet been achieved. The stoichiometry of the GaN needs to be investigated to reveal the compositions of the deposited films. Thus, the input levels of the reactant species can be properly controlled to create the best stoichiometric films. Also, because there is growth per cycle instead of a traditional growth rate, the rotation speed of the susceptor should be increase to quicken the layer-by-layer deposition process. Film depth versus rotational time correlations must be obtained to verify a true layer-by-layer process. Once monocrystalline GaN can be grown repetitively, attempts will be made to deposit different III-V nitride films in layers and finally in continuous solid solutions.

G. References

1. T. Suntola and J. Antson, U.S. Patent 4,058,430 (1977).
2. M. Ahonen, M. Pessa and T. Suntola, *Thin Solid Films*, **65**, 301 (1980).
3. M. Pessa, R. Makela and T. Suntola, *Appl. Phys. Lett.*, **38**, 131 (1981).
4. T. Yao and T. Takeda, *Appl. Phys. Lett.*, **48**, 160 (1986).
5. T. Yao, T. Takeda and T. Watanuki, *Appl. Phys. Lett.*, **48**, 1615 (1986).
6. T. Yao, *Jpn. J. Appl. Phys.*, **25**, L544 (1986).
7. T. Yao and T. Takeda, *J. Cryst. Growth*, **81**, 43, (1987).
8. M. Pessa, P. Huttunen and M.A. Herman, *J. Appl. Phys.*, **54**, 6047 (1983).
9. C.H.L. Goodman and M.V. Pessa, *J. Appl. Phys.*, **60**, R65 (1986).
10. M.A. Herman, M. Valli and M. Pessa, *J. Cryst. Growth*, **73**, 403 (1985).
11. V.P. Tanninen, M. Oikkonen and T. Tuomi, *Phys. Status Solidi*, **A67**, 573 (1981).
12. V.P. Tanninen, M. Oikkonen and T. Tuomi, *Thin Solid Films*, **90**, 283 (1983).
13. D. Theis, H. Oppolzer, G. Etchinghaus and S. Schild, *J. Cryst. Growth*, **63**, 47 (1983).
14. S. Lin, *J. Electrochm. Soc.*, **122**, 1405 (1975).
15. H. Antson, M. Leskela, L. Niinisto, E. Nykanen and M. Tammenmaa, Kem.-Kemi, **12**, 11 (1985).
16. R. Tornqvist, Ref. 57 in the bibliography of Chapt. 1 of Ref. 39 of this section.
17. M. Ylilammi, M. Sc. Thesis, *Helsinki Univ. of Technology*, Espoo (1979).
18. L. Hiltunen, M. Leaskela, M. Makela, L. Niinisto, E. Nykanen and P. Soininen, *Surface Coating and Technology*, in press.
19. I. Suni, Ref. 66 in the bibliography of Chapt. 1 of Ref. 39 in this section.
20. S.M. Bedair, M.A. Tischler, T. Katsuyama and N.A. El-Masry, *Appl. Phys. Lett.*, **47**, 51 (1985).
21. M.A. Tischler and S.M. Bedair, **48**, 1681 (1986).
22. M.A. Tischler and S.M. Bedair, *J. Cryst. Growth*, **77**, 89 (1986).
23. M.A. Tischler, N.G. Anderson and S.M. Bedair, *Appl. Phys. Lett.*, **49**, 1199 (1986).
24. M.A. Tischler, N.G. Anderson, R.M.Kolbas and S.M. Bedair, *Appl. Phys. Lett.*, **50**, 1266 (1987).

25. B.T. McDermott, N.A. El-Masry, M.A. Tischler and S.M. Bedair, *Appl. Phys. Lett.*, **51**, 1830 (1987).
26. M.A. Tischler, N.G. Anderson, R.M. Kolbas and S.M. Bedair, *SPIE Growth Comp. Semicond.*, **796**, 170 (1987).
27. S.M. Bedair in *Compound Semiconductor Growth Processing and Devices for the 1990's*, Gainesville, FL, 137 (1987).
28. J. Nishizawa, H. Abe and T. Kurabayashi, *J. Electrochem. Soc.*, **132**, 1197 (1985).
29. M. Nishizawa, T. Kurabayashi, H. Abe, and N. Sakurai, *J. Electrochem. Soc.*, **134**, 945 (1987).
30. P. D. Dapkus in Ref. 27, p. 95.
31. S.P. Denbaars, C.A. Beyler, A. Hariz and P.D. Dapkus, *Appl. Phys. Lett.*, **51**, 1530 (1987).
32. M. Razeghi, Ph. Maurel, F. Omnes and J. Nagle, *Appl. Phys. Lett.*, **51**, 2216 (1987).
33. M. Ozeki, K. Mochizuki, N. Ohtsuka and K. Kodama, *J. Vac. Sci. Technol.*, **B5**, 1184 (1987).
34. Y. Suda, D. Lubben, T. Motooka and J. Greene, *J. Vac. Sci. Technol.*, **B7**, 1171 (1989).
35. J. Nishizawa, K. Aoki, S. Suzuki and K. Kikuchi, *J. Cryst. Growth*, **99**, 502 (1990).
36. T. Tanaka, T. Fukuda, Y. Nagasawa, S. Miyazaki and M. Hirose, *Appl. Phys. Lett.*, **56**, 1445 (1990).
37. T. Suntola and J. Hyvarinen, *Ann. Rev. Mater. Sci.*, **25**, 177 (1985).
38. M. Simpson and P. Smith, *Chem. Brit.*, **23**, 37 (1987).
39. T. Suntola and M. Simpson, *Atomic Layer Epitaxy*, Chapman and Hall, New York, 1990.
40. H.P. Maruska and J.J. Tietjen, *Appl. Phys. Lett.*, **15**, 327 (1969).
41. W.M. Yim, E.J. Stofko, P.J. Zanzucchi, J.I. Pankove, M. Ettenberg and S.L. Gilbert, *J. Appl. Phys.*, **44**, 292 (1973).
42. J.A. Sajurjo, E. Lopez-Cruz, P.Vogh and M.Cardona, *Phys. Rev.*, **B28**, 4579 (1983).
43. J. Sumakeris, Z. Sitar, K.S. Ailey-Trent, K.L. More and R.F. Davis, *Thin Solid Films*, in press.
44. N. Kobayashi, T. Makimoto, and Y. Horikoshi, *Jpn. J. Appl. Phys.*, **24**, L962 (1985).
45. *Landolt-Bornsteinn*, Vol. 17, Springer, New York, 1982.

V. Luminescence of III-V Nitrides—Development of a Laboratory

A. Introduction

Luminescence is the emission of photons due to excited electrons in the conduction band decaying to their original energy levels in the valance band. The wavelength of the emitted light is directly related to the energy of the transition, by E=hv. Thus, the energy levels of a semiconductor, including radiative transitions between the conduction band, valance band, and exciton, donor, and acceptor levels, can be measured.[1,2]

In luminescence spectroscopy various methods exist to excite the electrons, including photoluminescence (photon excitation), and cathodoluminescence (electron-beam excitation). In each technique signal intensity is measured at specific wavelength intervals using a monochrometer and a detector. The intensity versus wavelength (or energy) plot can then be used to identify the characteristic energy band gap and exciton levels (Intrinsic luminescence) of the semiconductor, and the defect energy levels (extrinsic luminescence) within the gap.[1]

Both photo- and cathodoluminescence analysis has been performed on AlN, GaN, and $Al_xGa_{1-x}N$ semiconductors.[3-8] Much of the work has been in measuring the low temperature GaN luminescence peaks. Work on AlN has been limited by the energy gap of 6.2 eV, which corresponds to a wavelength (200 nm) that is lower than most of the optical light sources. An excimer laser using the ArF line (193 nm) can be used, but caution must be taken when operating at these wavelengths.

Few time-resolved luminescence measurements have been performed on AlN and GaN. In a time-resolved measurement a pulsed source is used to excite the sample, and the luminescence is measured at short sampling intervals after the pulse. The result is an intensity vs. time plot. Time resolved spectroscopy is useful for separating the emission bands of the investigated samples with different decay times. It is often used to measure donor-acceptor recombination rates and minority carrier lifetimes.[1]

Depth-resolved information can be obtained using cathodoluminescence, since generation depth varies with beam voltage. This technique is particularly useful for studying ion implanted semiconductors and layered structures.[1]

B. Future Research Plans/Goals

A combined photo- and cathodoluminescence system is currently being assembled. A schematic view is shown in Figure 1, and a block diagram is shown in Figure 2. The sample will be in a UHV chamber, and the monochrometer and collection optics will be in a vacuum environment. The sample will be attached to a cryostat from APD cryogenics, which will allow for luminescence measurements down to 4.2 K. The monochrometer is a McPherson model 219 vacuum monochrometer. Its focal length is .5 m, with a wavelength resolution of .04 nm at

313.1 nm. Two optical sources and a beam blanking electron gun will be used as the excitation sources. A He-Cd laser will first be used; it is a continuous wavelength laser that operates at wavelengths of 325 nm and 442 nm. A pulsed excimer laser is the other optical source; it operates at wavelengths of 193 nm (6.4 eV), 248 nm (5.0 eV), and 308 nm (4.0 eV); and so it can be used to measure the luminescence of AlN.

The beam blanking capability of the electron gun will make it possible to do time-delay studies of the semiconductors. A boxcar integrator will be used to collect the data. The electron gun will have maximum beam voltage of 15 keV, making it possible to perform depth-resolved spectroscopy.

Cathodoluminescence in the TEM will also be performed on the nitride films through a collaboration with Dr. Roger Graham at Arizona State University. In the TEM environment the luminescence from individual defects can be examined, and hence the source of extrinsic luminescence peaks can be identified.

The optical properties of the nitride films will be examined through a collaboration with Dr. Roger H. French of Du Pont. Reflectance and transmission measurements in the visible to the vacuum ultraviolet light range ($E \geq 40$ eV) are possible. Optical transmission measurements probe the fundamental absorption edge and determine the optical band gap energy. Reflectance measurements are useful for probing interband transitions lying at higher energies, where the material is opaque. Reflectance measurements also probe many-body excitations, such as exciton, and provide a valuable probe into how the electrons and holes interact in the lattice. VUV spectroscopy over a wide range (5 to 40 eV) allows one to exhaust the transitions of the intrinsic electronic structure and to determine the high-frequency dielectric constant and optical properties from Kramers-Kronig analysis. This provides a quantitative electronic structure information.[9] VUV spectroscopy has been performed on single crystal and polycrystalline AlN, but little has been done on AlN or GaN thin films.[10]

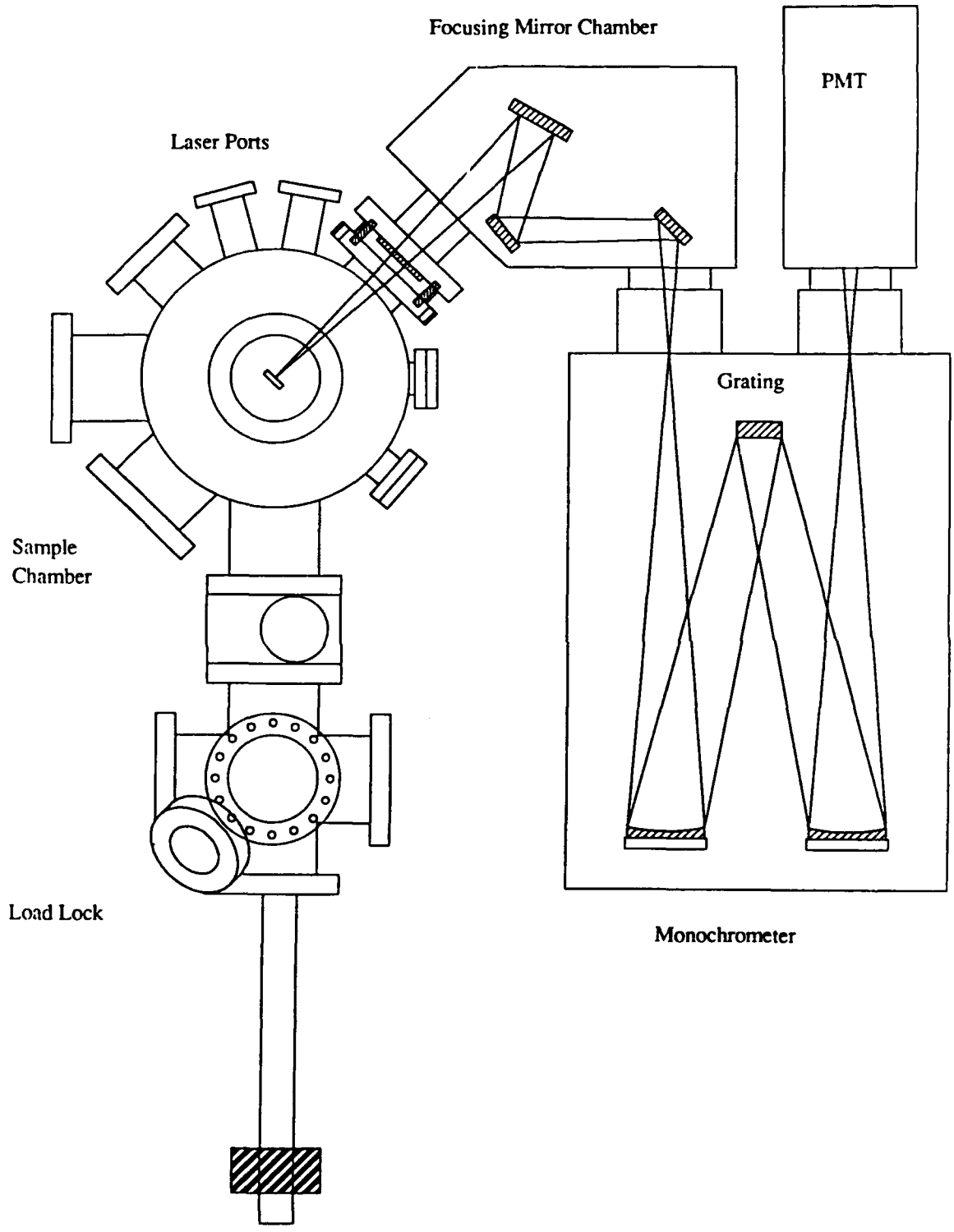

Figure 1. Schematic diagram of the photo-cathodoluminescence system.

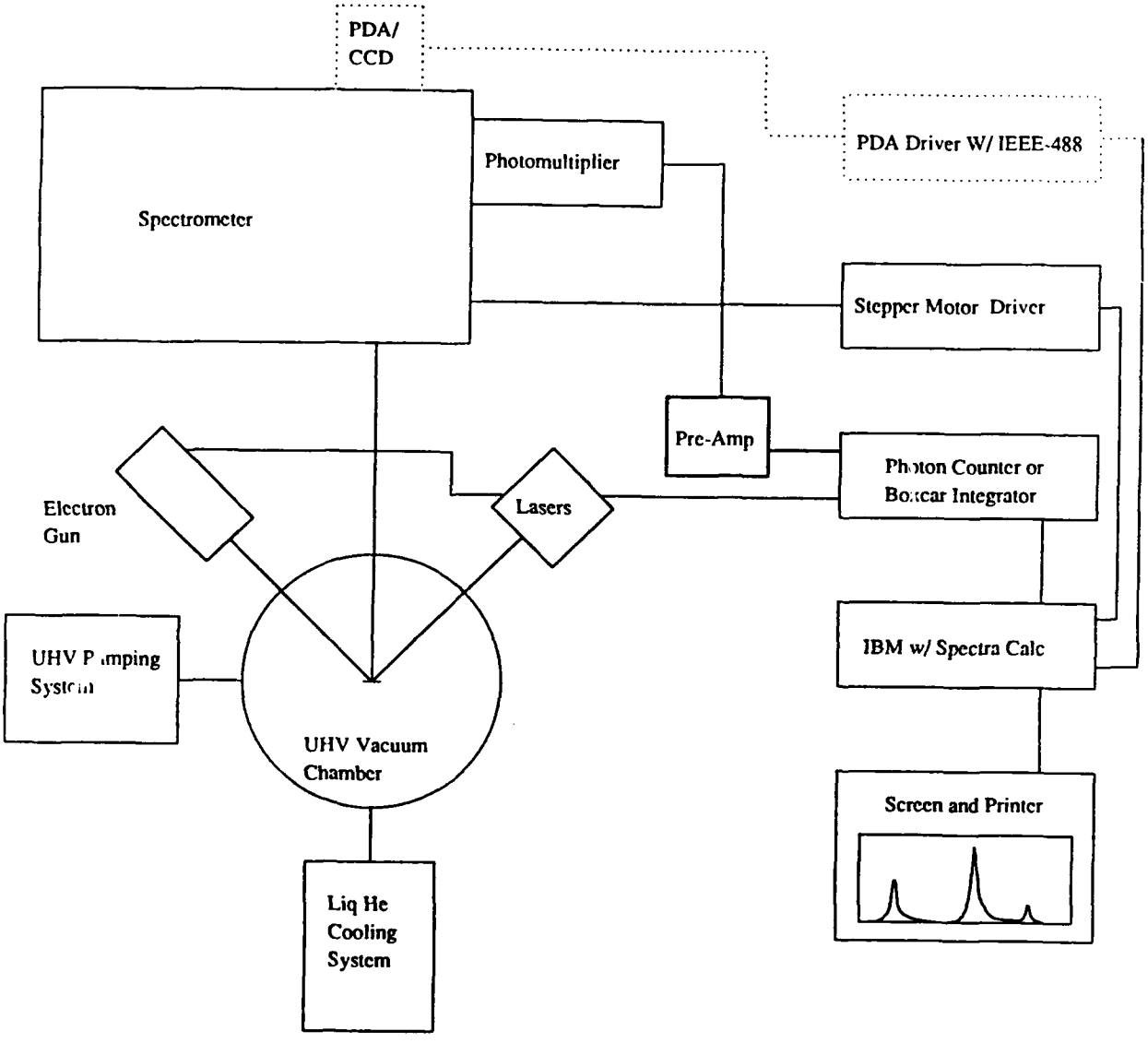

Figure 2. Block diagram of the photo-cathodoluminescence system.

VI. Impurity Doping and Contact Formation in GaN and AlN

A. Introduction

The III-V nitrides have long been known to possess properties that have potentially great technological value. These materials can be considered as largely covalent ceramics, whose unique combinations of properties are only beginning to be put to use. For electronic and optoelectronic device applications, the most important characteristics of the III-V nitrides are that they are all semiconductors having wide, direct band gaps and form complete solid solutions with one another. With the band gap of GaN being 3.4 eV and that of AlN 6.2 eV, the possibility exists for optical and optoelectronic devices active from the blue region of the electromagnetic spectrum to well into the ultraviolet. To date, semiconductor devices have been developed that operate in the infrared to green regions of the spectrum, but as yet attempts to push this capability to shorter wavelengths have been unsuccessful. The present study is part of an effort to characterize the semiconductor and optical properties of the III-V nitrides, and to demonstrate the valuable technological capabilities of these materials.

As part of this study, several dopant impurities (Si, Ge, C, Zn, and Mg) were implanted into GaN and AlN films grown by means of molecular beam epitaxy (MBE). These impurity species were selected as potential donors (Si, Ge), acceptors (Zn, Mg), or either (C) on the basis of their valences and the compatibility of their covalent radii with the wurtzite GaN and AlN lattices. Carbon, a Group IV element, is potentially amphoteric because it is possible for C to occupy either lattice site. Covalent radii, according to Van Vechten's model [1], of the elements involved in this study are listed in Table I.

Table I. Tetrahedral covalent radii of selected elements, according to Van Vechten [1]

Element	r (Å)
Al	1.230
Ga	1.225
N	0.719
Si	1.173
Ge	1.225
C	0.774
Zn	1.225
Mg	1.301

After the incorporation of the dopant species, rapid thermal annealing (RTA) steps were performed to investigate the effect of annealing treatment on dopant activation. The RTA technique was chosen for these experiments because the short time spent at high temperature in the process would minimize the loss of nitrogen from the films and thus minimize the formation of N vacancies. Nitrogen vacancies are defects that act as electron donors in these crystals; their presence would contribute to obscuring the effects of dopant activation.

Surface cleaning and oxidation studies of GaN and AlN will shortly be conducted, prior to systematic investigations of ohmic contact formation to these materials.

B. Experimental Procedure

1. Ion Implantation

For this study GaN and AlN films were grown at NCSU by means of gas source MBE on α-SiC single crystal substrates supplied by Cree Research. The MBE growth system is described in more detail in another section of this report. The GaN and AlN films were grown to thicknesses of 3000Å and 4000Å, respectively. These GaN and AlN layers were then implanted with ^{29}Si, ^{74}Ge, ^{12}C, ^{66}Zn, and ^{24}Mg at the Surface Modification and Characterization Facility at Oak Ridge National Laboratory. Implantation of the dopant species was conducted in two steps: one step to a peak depth of 750-800Å, and a second step to peak at a depth of 80-110Å. Such a combination of implantation steps would produce an approximately flat dopant profile through most of the total implantation depth. Projected implant concentration profiles were calculated using a software program named PROFILE (Version 3.18, Implant Sciences Corporation, Wakefield, MA). Ion implantation energies were varied with the implant species and the target materials so as to maintain similar depth profiles. Implant doses were varied to achieve peak atomic volume concentrations of 10^{19} and 10^{20} cm^{-3}. The implantation was conducted at a target offset angle of 5° to minimize channeling effects on the incident beam. In addition, the samples were heated to 500°C during implantation to provide a certain amount of self-annealing and activation of the dopant during the implantation process. In a previous study of implantation of SiC [2], it was found that implanting SiC targets at elevated temperature resulted in improved dopant activation. Implantation temperatures above 500°C did not result in significant further increases in dopant activity.

2. Rapid Thermal Annealing

After implantation the samples' resistivities were measured prior to RTA treatment. Annealing steps were conducted in a Heatpulse 210 model (AG Associates) rapid thermal annealing furnace under 1 atm N_2. The GaN samples were treated with 10 s annealing steps at 1000°C; the AlN samples were treated at 1100°C, also for 10 second steps.

3. Electrical Measurements

The electrical resistance of each specimen was measured by means of current-voltage data acquired by a pair of surface probes using a Hewlett Packard 4145A Semiconductor Parameter Analyzer system. This method does not provide an accurate measurement of a material's inherent resistivity; the measured resistance includes, for example, any contact resistance between the probe tip and the film surface. This method does, however, provide a means of comparing the behavior of samples to one another when the measurements are taken with a consistent procedure. For this study the surface probes were placed at a consistent separation distance of 1 mm near the center of each specimen. Four point probe measurements are more commonly used to characterize the resistivities of more conventional semiconductors, but the nitride films used in this study were too resistive for accurate detection using this method. For the same reason it was not possible to obtain accurate Hall effect measurements of most of the samples for the evaluation of electrical carrier types and concentrations.

C. Results

Prior to implantation, the as-grown GaN and AlN films were highly resistive. The term "highly resistive" used here means that a sample's resistance as measured by the surface probe current-voltage (I-V) method was beyond the sensitivity of the instrument, which corresponds to a resistance of approximately 10^{12} Ω. The measured resistance values varied across the surfaces of most of the samples; for the more resistive films (10^{8}-10^{12} Ω range) this variation was considerable - as much as 100 percent in some cases. The results of the I-V measurements are listed in Tables II and III. The results of Mg implantation are not listed, as the second implantation step had not been completed by the time of the writing of this report. The same applies to the second annealing step for the C-doped samples.

After the two-step implantation sequences were completed, all the tested films were still highly resistive. After one 10-second RTA step at 1000°C, however, the GaN films began to show some measurable decrease in resistance. At this point, the Si-doped and Zn-doped GaN films had similar resistances in the 2×10^{7} Ω range, while the Ge-doped films exhibited much higher resistance (8×10^{10} Ω). Interestingly, the less-highly doped C:GaN (N=10^{19} cm^{-3}) films showed a significant decrease in resistance while the N=10^{20} cm^{-3} films remained highly resistive. The AlN films remained highly resistant throughout.

Table II. Compared resistances (in Ω) of GaN and AlN films implanted with Si and Ge

	Doping Level (cm^{-3})	Si:GaN	Si:AlN	Ge:GaN	Ge:AlN
As Grown	10^{19}		HR		HR
	10^{20}	HR*	HR	HR	HR
As Implanted	10^{19}		HR		HR
	10^{20}	HR	HR	HR	HR
(1) 10 s	10^{19}		HR		HR
RTA step	10^{20}	2.63×10^{7}	HR	8.2×10^{10}	HR
(2) 10 s	10^{19}		HR		HR
RTA steps	10^{20}	2.14×10^{6}	HR	1.0×10^{11}	HR

* HR = highly resistive ($>10^{12}$ Ω)

Table II. Compared resistances (in Ω) of GaN and AlN films implanted with C and Zn

	Doping Level (cm^{-3})	C:GaN	C:AlN	Zn:GaN	Zn:AlN
As Grown	10^{19}	HR*		HR	
	10^{20}	HR	HR	HR	HR
As Implanted	10^{19}	HR		HR	
	10^{20}	HR	HR	HR	HR
(1) 10 s	10^{19}	5.8×10^{9}		HR	
RTA step	10^{20}	HR	HR	1.5×10^{7}	HR
(2) 10 s	10^{19}	†		HR	
RTA steps	10^{20}	†	HR	1.9×10^{7}	HR

* HR = highly resistive ($>10^{12}$ Ω)
† Measurements not yet completed

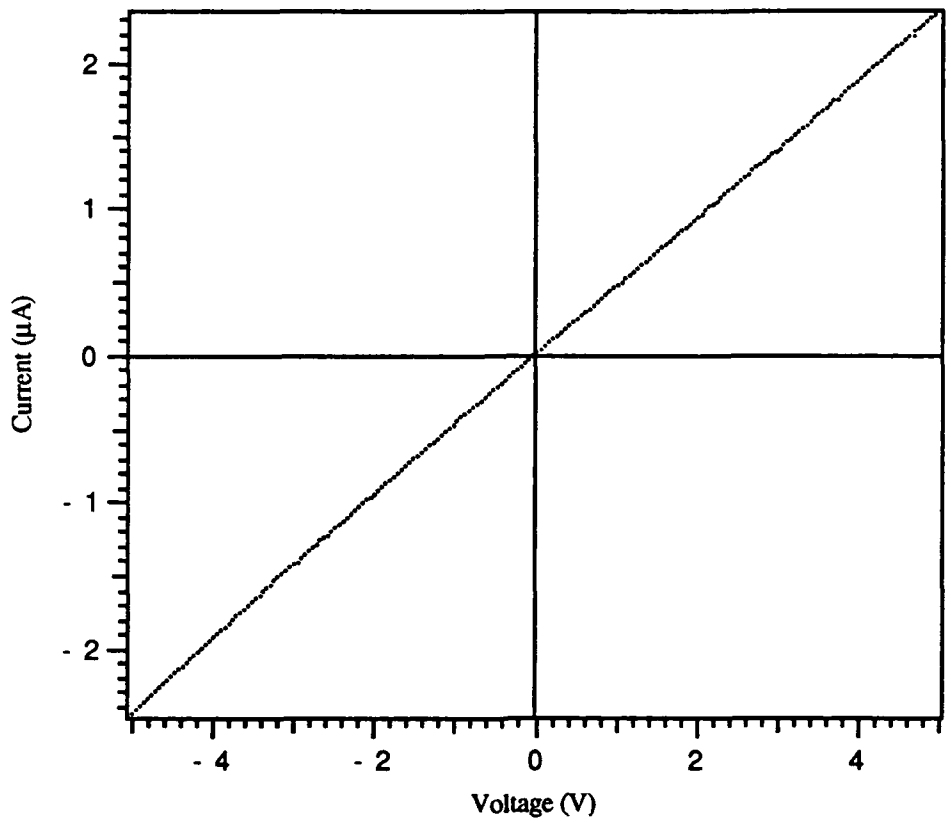

Figure 1. Current-voltage measurement of Si:GaN ($N=10^{20}$ cm^{-3}) after two 10 s RTA steps at 1000°C.

After a second annealing step, the Ge:GaN and Zn:GaN films had not changed appreciably. The Si:GaN $N=10^{20}$ cm^{-3} film, however, revealed a decrease in resistance of another order of magnitude. The I-V plot for this sample is shown in Figure 1, and indicates a simple linear, ohmic I-V relationship. The resistance of the circuit is represented by the slope of the line, using Ohm's law (R=V/I). Such a plot was typical of all measurements below about 10^9 Ω. Measurements of higher resistances did not have completely linear I-V relationships; in these cases the slopes of the most linear regions of the plots (at lower values of V) were used. The Si:GaN $N=10^{20}$ cm^{-3} film supported a current of almost 2.5 μA at +5 V; this film was conductive enough for Hall effect measurements, which yielded an n-type carrier concentration of 1.574×10^{17} cm^{-3} and a Hall mobility of 11.064 $cm^2/V\cdot s$. However, due to a high contact resistance between the indium contacts and the film, these measurements were not very accurate. This and other films may gain sufficient charge carrier transport for four-point probe measurements and better Hall measurements after additional annealing steps. Steps will be taken to improve the contact quality for Hall measurements.

D. Discussion

Among the films tested to date, the Si:GaN sample having a doping level of 10^{20} cm^{-3} exhibited the greatest reduction in surface resistance. This film's resistance was reduced from being too high to measure to 2×10^6 Ω after two 10 s rapid annealing steps at 1000°C. The Hall effect measurement revealed the conductivity to be n-type, which would result from the Si atoms occupying the Group III sites and acting as electron donors. Both Si and Ge are Group IV elements, along with C, and so have amphoteric valence in a III-V lattice. Previous studies of Group IV doping of GaN [3,4] were conducted in an attempt to observe p-type conductivity as a result of the Group IV element occupying vacant N sites, but these attempts were not successful. The fact that a silicon nitride (Si_3N_4) forms a well-bonded, stable compound contributes to the likelihood that Si may substitute in the Group III site. In addition, the fact that Si forms a more stable nitride than does Ge may allow Si to bond more securely with the nitride lattice and thus be more easily activated as a dopant than Ge. The apparent lack of significant Ge activation may be due to Ge not bonding well with the nitride lattice, and also to the fact that Ge^+, being a significantly heavier ion than Si^+, caused more lattice damage during implantation than did Si^+. The elevated temperature of the target during implantation (500°C) should have helped reduce lattice damage, but it may be that higher implantation temperatures would be more effective, particularly for AlN.

Zinc is also a heavy atom compared to the others involved in this study, and thus would also cause more damage than the others during implantation. The Zn:GaN film ($N=10^{20}$ cm^{-3}) showed a significant decrease in resistance after one annealing step, but not with another anneal. Magnesium may turn out to give better results than Zn; it is a less massive particle than Zn and it has already been demonstrated to create p-type doping when activated with electron beam irradiation [5,6].

It has been frequently observed that successful p-type doping of III-V and II-VI compounds is difficult [7-9]. This problem has been attributed to the semiconductor lattice compensating for the acceptor impurities by generating crystal defects that act as donors and have relatively low energies of formation - in this case N vacancies. The fact that the C:GaN film in which $N=10^{19}$ cm^{-3} showed a significant decrease in resistance, whereas the more heavily doped film did not, may be due to overdoping or the C being over its solubility limit in the matrix. Neumark *et al.* [8,9] point out that, fundamentally, an impurity's lack of solubility in a semiconductor is the reason behind the difficulty in activating the impurity as a dopant. However, at the present time impurity solubilities in these nitride materials have not been widely studied; it is planned in this investigation to estimate the solubilities of the various dopants on the basis of available phase diagrams and literature. In addition, it has been claimed as a result of luminescence studies [10] that C in GaN creates a deep acceptor level (860 meV

above the valence band edge) and thus in high concentrations may act more as electron traps than as acceptors that contribute to charge transport.

Overall, it is likely that these nitride crystals will exhibit better electronic properties when film quality has been improved further. Cross-sectional TEM images of films similar to the ones grown for this doping study have shown an unexpectedly large number of structural defects such as low-angle boundaries, which could be responsible for impeding charge carrier transport in general and thereby increasing the observed resistance of the films. Efforts are currently underway to improve the film deposition process.

E. Conclusions

Silicon doping of GaN films, activated by RTA treatment, has been shown to significantly reduce film resistance. Zinc and C doping reduced film resistance to a lesser degree, due possibly to charge compensation, solubility limitations, or both. The effect of Ge doping was only barely noticeable. All the AlN films remained highly resistive throughout. It is possible that additional annealing treatments will produce further improvement in properties; better film quality, as well, should have a beneficial effect. Further decreases in film resistance will allow more accurate measurement of film resistivities and Hall effect measurements, which will reveal the charge carrier types and concentrations.

F. Future Plans/Goals

The investigation of p- and n-type dopant activation will continue. Additional RTA steps will be performed and more detailed electrical characterization will be conducted as the films become sufficiently less resistant. As film quality improves, it is expected that the effects of impurity addition and dopant activation will be more pronounced and accurately determined. Photoluminescence and cathodoluminescence spectroscopy examinations will be performed in an effort to characterize the electronic energy level structures of these materials and identify states corresponding to structural defects and impurity species. In addition, studies of ohmic contact formation to these nitride films will be conducted. Forming good ohmic contacts is a fundamentally important technological step in the fabrication of working semiconductor devices.

Extensive coverage of ohmic contact formation to GaAs can be found in the literature; studies of other III-V semiconductors are much fewer, although some work on GaN has been reported [11,12]. The preceding Semiannual Report for this work includes discussion of some important considerations in the search for ohmic contact materials. Indium as an ohmic contact for n-type nitride films and Pt as an ohmic contact for p-type will receive the most emphasis initially, on the basis of their chemical relationship with the nitride crystals and their work functions relative to those of GaN and AlN, according to the Schottky-Mott-Bardeen model.

Multiple avenues of this subject will be explored, including the effects of subsequent annealing on the contact behavior, cross-sectional examination of interfaces via transmission electron microscopy (TEM), and probing the metal-semiconductor surface using spectroscopic techniques such as x-ray photoelectron spectroscopy (XPS).

It is also planned to investigate the effects of various surface cleaning procedures and oxidation conditions, in order to identify effective surface preparation strategies. In the formation of reproducible ohmic contacts, it will be necessary to minimize interfacial contamination and surface nonuniformities. In addition to comparing cleaning procedures, it will also be useful to better characterize the oxidation of these thin nitride films, especially AlN. Various studies have been published describing the oxidation of different forms of AlN, from fine powders to hot-pressed solids [13-16], but as yet little information is available concerning single crystal or near single crystal films. Oxide films can be either useful or detrimental for semiconductors, depending on the chemical and physical natures of the materials involved. Characterization of the surface oxidation of the III-V nitrides will be a constructive step in the understanding and implementation of these unique materials.

G. References

1. J. A. Van Vechten, J.C. Phillips, Phys. Rev. B **2**(60), 2160 (1970).
2. J.A. Edmond, S.P. Withrow, W. Wadlin, and R.F. Davis in *Interfaces, Superlattices and Thin Films*, edited by J.D. Dow and I.K. Schuller (Mater. Res. Soc. Proc. **77**, Pittsburgh, PA 1987) p. 193.
3. H.P. Maruska, J.J. Tietjen, Appl. Phys. Lett. **15**, 327 (1969).
4. R.D. Cunningham, R.W. Brander, N.D. Knee, D.K. Wickenden, J. Luminescence **5**, 21 (1972).
5. H. Amano, M. Kito, K. Hiramatsu, I. Akasaki, Japan. J. Appl. Phys. **28**(12), L2112 (1989).
6. I. Akasaki, H. Amano, M. Kito, K. Hiramatsu, J. Luminescence **48&49**, 666 (1991).
7. C.H.L. Goodman, Mat. Res. Bull. **20**, 961 (1985).
8. G.F. Neumark, Phys. Rev. Lett. **62**, 1800 (1989).
9. D.B. Laks, C.G. Van de Walle, G.F. Neumark, S.T. Pantelides, Phys. Rev. Lett. **66**, 648 (1991).
10. T. Ogino, M. Aoki, Japan. J. Appl. Phys. **19**, 2395 (1980).
11. T. C. Shen, G. B. Gao, H. Morkoç, J. Vac. Sci. Technol. B **10**(5) 2113 (1992).
12. J.S. Foresi, *Ohmic Contacts and Schottly Barriers on GaN*, M.S. thesis, Boston University (1992).
13. A.D. Katnani, K.I. Papathomas, J. Vac. Sci. Technol A **5**(4), 1335 (1987).
14. D. Suryanarayana, J. Am. Ceram. Soc. **73**(4), 1108 (1990).
15 T. Sato, K. Haryu, T. Endo, M. Shimada, J. Mater. Sci. **22**, 2277 (1987).
16. D. Suryanarayana, L.J. Matienzo, D. Spencer, IEEE Trans. Comp., Hybrids, Manuf. Technol. **12**(4), 570 (1989).

VII. Reactive Ion Etching of GaN and AlN

A. Introduction

Semiconductor devices are the principle components of electronic and telecommunications systems [1]. In order to densely pack these microscopic components, unidirectional, or anisotropic, etching techniques are required to produce a fine network of lines. Wet etching processes found in many semiconductor manufacturing steps produce a multi-directional, or isotropically, etched material. This is undesirable for microcircuitry since the goal is to produce the smallest devices possible. Therefore, plasma-assisted processes, such as reactive ion etching (RIE), combine the physical characteristics of sputtering with the chemical activity of reactive species to produce a highly directional feature. RIE has the added advantage of providing a more uniform etch and a higher degree of material etch selectivity.

RIE has been employed to etch a wide variety of semiconductor materials including silicon-based materials [2-11], metals, like aluminum [3, 12-18] and III-V compounds, such as GaAs and InP [19-21]. However, plasma-assisted etching of newer III-V compounds, such as GaN and AlN, has been attempted by few investigators [20, 21]. There has been wide spread interest in using these nitrides for semiconductor device applications requiring visible light emission, high temperature operation and high electron velocities [20]. Since these materials possess wide bandgaps and optical emissions spectra in the blue to near ultraviolet range, they are prime candidates for ultraviolet detection devices.

The objectives of this report are to discuss recent progress made in the field of reactive ion etching of gallium and aluminum nitride. A long term goal is to develop and characterize suitable processes for the anisotropic etching of these nitrides. In the following sections, a brief review of pertinent literature on plasma-assisted etching of gallium and aluminum compounds is provided along with an outline of proposed research efforts.

B. Literature Review

Reactive Ion Etching of GaN. Since GaN is a direct transition material with a bandgap ranging from 3.4-6.2 eV at room temperature, it is an ideal candidate for the fabrication of shortwave length light emitters [20, 22]. High quality GaN films have been successfully grown by MOVPE [22], ECR-MBE [23, 24], MOCVD [25] and a layer-by-layer process [26] on a number of substrate. In order to fabricate complete device structures, reliable etching processes need to be developed. Since GaN is nearly inert to most wet etching solutions, with the exception of highly concentrated hot NaOH and H_2SO_4 [27], RIE may prove to be an effective method for the production of fine line patterning in semiconductor materials.

Recently, there have been a few attempts at etching GaN by plasma-assisted processes [20, 21]. Foresi [21] investigated fabrication techniques for ohmic contact and schottky barriers on

GaN. One of the highlights of his work was the successful etching of GaN on sapphire substrate in Freon 12 (CCl_2F_2) and in hydrogen atmospheres operating at about 10 mtorr and 40 and 60 W of RF power. Results from SEM photographs showed that in the CCl_2F_2 plasma, GaN had been completely removed from areas that were not covered by photoresist, and that the sapphire substrate was nearly unetched. Foresi was able to obtain an etch rate of approximately 140 Å/min in the CCl_2F_2 plasma at 60 W, while the hydrogen plasma produced insignificant etching results. Etch selectivity between the GaN and photoresist was found to be 3:1.

In another investigation, conducted by Tanaka et al. [20] reactive fast atom beam etching was employed to etch GaN on sapphire in a Cl_2 plasma at substrate temperatures ranging between 80-150°C. Etch rates of 1000-1200 Å/min produced relatively smooth surfaces and a well defined pattern of elongated rectangular bars on the sapphire.

Reactive Ion Etching of AlN. Aluminum nitride is a candidate material for optoelectronic devices because it possess a high electrical resistivity, high thermal conductivity, low dielectric constant and has a direct transition bandgap of 6.3 eV [28]. AlN films have been grown by several techniques including CVD, MBE and ALE, and on a variety of substrate materials including sapphire, silicon, spinel, silicon carbide and quartz [29]. Etching fine features in the AlN films is an important step in the fabrication of such devices. Though, no reports of etching of AlN are available in the open literature at this time, much work has been conducted on etching of metallic aluminum thin films [3, 12-18]. As a result, analogies to well established data for etching of aluminum are made. Although aluminum and AlN are very different materials, the chemistry and reactions in the plasma may be similar. So, it is proposed that reactive ion etching may also be an effective means for the application of fine line patterning of AlN.

A review of the literature shows that there are two primary methods employed for etching aluminum. Bruce and Malafsky [12] employed a parallel plate configuration (RIE) to investigate the effects of Cl_2 on aluminum. They found that two processes are involved, namely, the removal of the oxide layer and etching the metal below it. For those experiments, it was hypothesized that BCl_3 gas was necessary for the removal of the oxide layer because it was responsible for the initiation of a reduction reaction with the oxide. In the RIE etching configuration, aluminum etched with a chlorinated gas is a purely chemical reaction with little contribution from ion bombardment. This conclusion was made as a result of the insensitivity of RF power to the etch rate [12]. Therefore, anisotropic etching was thought to have been the result of a sidewall passivation mechanism whereby a protective layer is formed on the vertical walls of the trench by reaction of H_2O or carbon containing species with the aluminum. Since ion bombardment is normal to the surface, the walls remained unetched. This mechanism was produced by the addition of $CHCl_3$ to the mixture of gases. Feature widths of 2.25 μm were

produced by a gas mixture of Cl_2, BCl3, $CHCl_3$ and He at about 1.2 mtorr. Helium gas was added to the mixture to reduce the amount of erosion of the photoresist.

The combination of an isotropic flux of reactive species with a highly directional beam of energetic ions, so called ion beam assisted etching (IBAE), has been employed for the anisotropic etching of aluminum by many investigators [13-15, 18]. For IBAE, the aluminum oxide layer can be physical removed by sputtering with Ar^+ or Xe^+ ions, whereas with RIE the oxide is removed chemically [13]. However, etching takes place again by chemical reaction of Cl_2 with the aluminum as determined by the lack of dependence of the etch rate on the ion energy and current [14, 15]. From a mechanistic point of view, Cl_2 adsorbs onto and diffuses into the aluminum resulting in the formation of aluminum chlorides. Al_2Cl_6 is the dominant etch product at lower temperatures (33°C), while $AlCl_3$ was observed at higher temperatures (210°C) [15]. Saturation of the etched surface with chlorine atoms occurs prior to desorption of $AlCl_3$.

The etch rate is dependent upon several parameters including the presence of residual gases in the chamber, substrate temperature, Cl_2 flux, ion beam and the presence of carbon containing species. Impurity gases in the chamber (i.e. H_2O, O_2, N_2, etc.) can react with the aluminum films and impede the etching process by leaving a residue on the etched surface. This reduces the amount of Cl_2 available for reaction and consequently lowers the etch rate [13]. The substrate temperature is another parameter that affects the etch rate of aluminum. Efremow et al. [13] observed a two-fold increase in the etch rate by heating the substrate from 0° to 100°C. It was hypothesized that the increase in temperature led to a higher evaporation rate of the product $AlCl_3$. In addition, they found that an increase in the Cl_2 flux produced a significant amount of undercutting due to the nondirectional flow of the Cl_2 gas. A higher degree of anisotropy was achieved by the combination of ion beam and Cl_2 flux. Efremow et al. suggested that sidewall passivation (by reaction of H_2O with the aluminum) was partly responsible for the production of the very fine features in their samples. Submicrostructures of 80 nm wide lines were etched into a 100 nm thick aluminum film with 0.3 mtorr Cl_2 gas and 0.1 mA, 1 keV Ar^+ beam. Lastly, Parks et al. [14] found that chemisorption of the halocarbon gas molecules, such as CCl_4 and CBr_4, onto the aluminum surface formed halogentated aluminum species along with an aluminum carbide. Therefore, a significant reduction in the etch rate was observed due to the difficulty encountered in removing the carbide from the surface.

Oxidation of Aluminum Nitride. Previously, it was mentioned that an important step in etching aluminum is the removal of the oxide layer. This may also be an important first step in the etching of AlN since the existence of an oxide layer on AlN is well documented [30-34]. It has been shown that AlN is thermodynamically unstable in oxygenated environments at temperatures exceeding 700°C [31-34]. XPS and X-ray diffraction analyses [34] show the presence of a porous ALON intermediate layer produced during thermal oxidation at

temperatures greater than 700°C, while the combination of pressure and high temperature results in an AlOOH interlayers. In addition, at higher temperatures (> 1100°C), there appeared to be oxygen saturation of the oxide layer after which point no weight gain was observed [34]. This is highly indicative of the formation of a protective layer, such as Al_2O_3, which inhibits further formation of the oxide. Variations in the oxidation temperatures of AlN have been reported [31-34] and may be the result of variations in the grain size, porosity, impurity content and humidity levels [33]. Lastly, the following oxidation mechanism for AlN was proposed by Suryanarayana et al. [34]. As a result of the brittle nature of AlN, stresses and strains produced via the difference in thermal expansion coefficients between the oxide and nitride cannot be accommodated by the microstructure without the formation of microcracks and micropores. These defects seem to be generated in the oxide layer. Thus, nitrogen is liberated form the surfaces of the cracks and oxygen can diffuse to the surface of the oxide scale. The formation of Al_2O_3 on the nitride surface results in passivation and inhibits the diffusion of the oxygen to the surface at higher temperatures.

C. Proposed Research

Experimental Apparatus. A schematic diagram of the proposed RIE system is shown in Figure 1. The design of this system is based on that of the standard parallel-plate diode configuration in which the bottom electrode is powered by a RF power supply (see for example Ref. 10). The apparatus in this design consists of a stainless steel chamber and a water-cooled steel or aluminum electrode. These materials were chosen for their ability to resist chemical attack from the process gases. During the etching process, the samples will be placed on the bottom electrode which may be coated with graphite (or an equivalent material) to prevent sample contamination. Mass flow controllers are desirable for the accurate and safe control of the process gases.

The pumping system consists of a diffusion pump and cold trap combined with a mechanical pump. A control valve is used to maintain a prescribed processing pressure in the chamber during etching runs, while additional flexibility in the range of processing pressures is ensured by the presence of two isolation valves.

A 13.56 MHz RF power supply with a dual capacitance matching network is connected to the electrode to maintain a glow discharge between the electrodes. It is likely that a power range of 0-300 W will be required for these experiments for maximum flexibility.

In addition, a mass spectrometer (or equivalent apparatus) can be employed for the detection and characterization of chemical species produced by and during the etching process. It is hoped that this analytical instrumentation will provide necessary information for the determination of the success of the etching processes and will provide a basis for an understanding of the etching mechanisms.

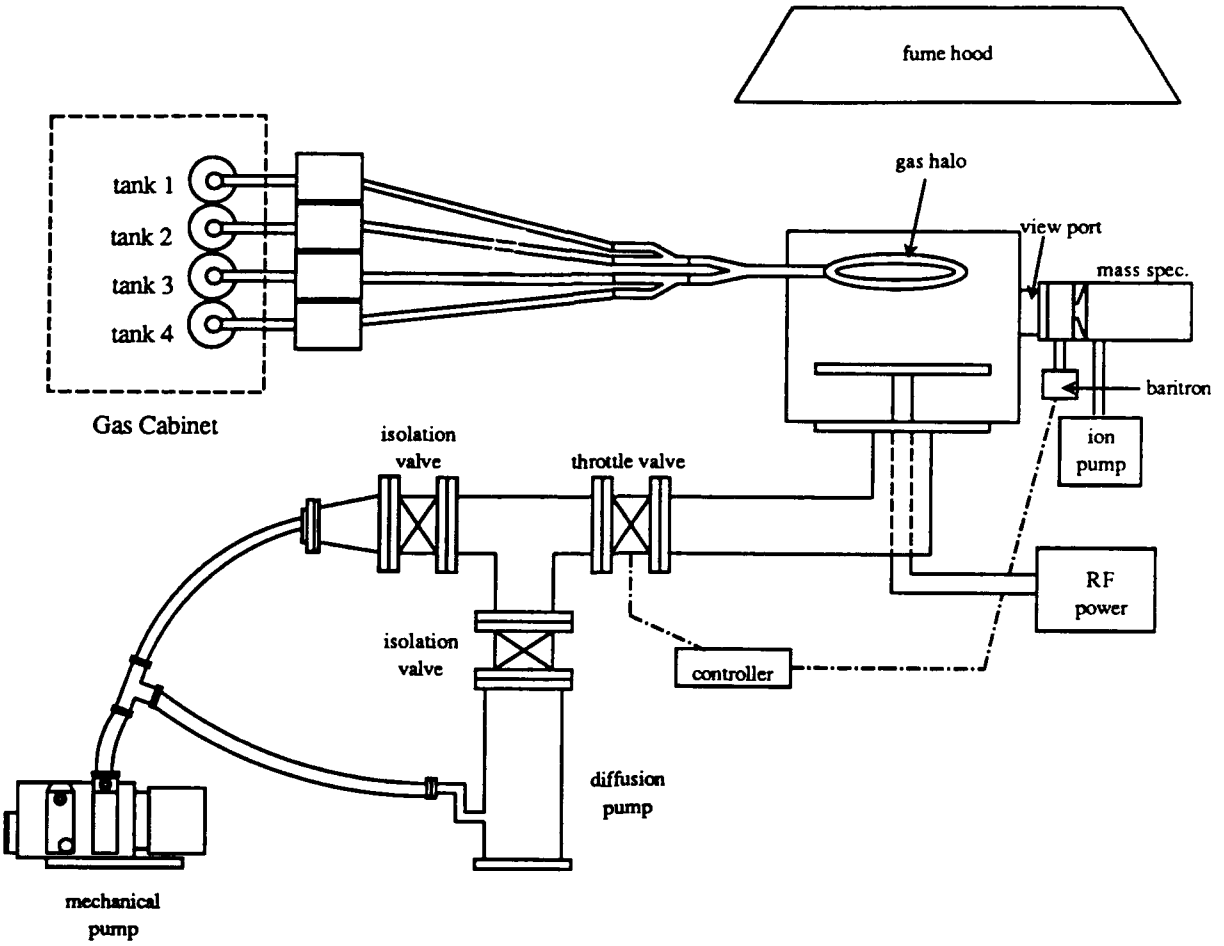

Figure 1. Proposed RIE system design (drawing not to scale).

Choice of Process Gases. There are a number of process gases that can be used for anisotropic etching of GaN and AlN. Fluorine plasmas are impractical for etching aluminum and gallium compounds because involitile fluorides are formed at the surfaces, therefore limiting desorption or reaction species from the surface [35]. Chlorine plasmas, on the other hand, have been used extensively for etching aluminum and gallium compounds, see Section B above. The following points [36] will also be considered in choosing the process gases:

1. Mixed halogen etching gases containing Cl and Br are often used for anisotropic etching, e.g. $CClF_3$, CCl_2F_2, CCl_3F, and CF_3Br. The concentration of Cl and Br can be increased by adding O_2 to the mixed halocarbon gases. However, this could enhance polymerization of the chamber walls, electrodes and substrate.

2. Sidewall passivation layers, i.e. polymerized films, are important in achieving etch directionality in many dry etching processes. The glow discharge chemistry should be chosen so that etch inhibiting films can form as long as they are not exposed to ion bombardment, which leads to the dissolution of films. Conceptually, it appears that

sidewall passivation forming gases (such as O_2 and H_2) can be added directly to the primary etching gases of which the amount of sidewall passivation can be controlled by the mixing ratio. However, the addition of such gases can change the etch rate and masking selectivity of the process.

3. The addition of O_2 to Cl and Br plasma gases tends to increase the atomic concentration of Cl and Br in the plasma and reduce the amount of polymerization.

4. The addition of H_2 to Cl and Br plasma gases has a tendency to reduce the atomic concentration of Cl and Br thus increasing the amount of polymerization.

5. The addition of Ar and other noble gases to the plasma has a tendency to stabilize the plasma or can be used for cooling purposes (He can be used for high pressure gases). Ar can also cause inert ion bombardment of the surface and aid in producing anisotropic etching.

In etching GaN, the gases used for the investigations of Tanaka [20] and Foresi [21], namely CCl_2F_2 and Cl_2, will be employed first since those investigators reported successful results. Experimentation with other combinations of gases is likely in order to obtain anisotropic features and reasonably high etch rates. As for AlN, chlorine containing gases with additions of O_2, carbon containing gases and or noble gases (i.e. Ar, He, etc.) are likely candidate gases. Though, somewhat of a trial and error methodology will be followed until success is achieved. It is noted that for RIE, sidewall passivation is an important mechanism for anisotropic etching and will generally produce larger features. On the other hand, ion beam assisted etching, or similar techniques, are likely to produces smaller features in these nitrides.

D. Future Research

Future plans include the acquisition and installation of a RIE system similar to the one shown in Figure 1, the development and characterization of suitable etching processes for aluminum and gallium nitride and the additional research on the chemistry and thermodynamics of these processes.

E. References

1. *Plasma Processing of Materials: Scientific Opportunities and Technological Challenges*, Panel on Plasma Processing of Materials, National Research Council (National Academy Press, Washington, D.C., 1991).
2. J. W. Palmour, R. F. Davis, T. M. Wallett and K. B. Bhasin, *J. Vac. Sci. Technol.*, **A4**, 590 (1986).
3. D. L. Smith, P. G. Saviano, *J. Vac. Sci. Technol.*, **21**, 768 (1982).

4. D. L. Smith and R. H. Bruce, *J. Electrochem. Soc.*, **129**, 2045, (1978).
5. C. J. Mogab, A. C. Adams and D. L. Flamm, *J. Appl. Phys.*, **49**, 3796 (1978).
6. S. Matsuo, *J. Vac. Sci. Technol.*, **17**, 587 (1980).
7. L.M. Ephrath, *Solid State Technol.*, July 1982, p. 87.
8. Y. H. Lee and M. M. Chen, *J. Appl. Phys.*, **54**, 5966 (1983).
9. L. M. Ephrath, *J. Electrochem. Soc.*, August 1979, p. 1419.
10. A. J. van Roosmalen, *Vacuum*, **34**, 429 (1984).
11. M. Zhang, J. Z. Li, I. Adesida and E. D. Wolf, *J. Vac. Sci. Technol.*, **B1**, 1037 (1983).
12. R. H. Bruce and G. P. Malafsky, *J. Electrochem. Soc.*, **136**, 1369 (1983).
13. N. N. Efremow, M. W. Geis, R.W. Mountain, G.A. Lincoln, J.N. Randall and N.P. Economou, *J. Vac. Sci. Technol.*, **B4**, 337 (1986).
14. S. Park, L. C. Rathburn and T. N. Rhodin, *J. Vac. Sci. Technol.*, **A3**, 791 (1985).
15. H. F. Winters, *J. Vac. Sci. Technol.*, **B3**, 9 (1985).
16. D. A. Danner and D. W.Hess, *J. Appl. Phys.*, **59**, 940 (1986).
17. R. J. A. A. Janssen, A. W. Kolfschoten and G. N. A. van Veen, *Appl. Phys. Lett.*, **52**, 98 (1988).
18. Y. Ochiai, K. Shihoyama, T. Shiokawa, K. Toyoda, A. Masuyama, K. Gamu, S. Namba, *J. Appl. Phys.*, **25**, L527 (1986).
19. G. Smolinski, R. P. Chang and T. M. Mayer, *J. Vac. Sci. Technol.*, **18**, 12 (1981).
20. H. Tanaka, *Optoelectronics - Devices and Technologies*, **6**, 150 (1991).
21. J. S. Foresi, *Ohmic Contacts and Schottky Barriers on Gallium Nitride*, M.S. Thesis (Boston University, Department of Electrical, Computer and Systems Engineering, Boston, MA, 1992).
22. I. Akasaki and H. Amano, "Conductivity control of AlGaN, fabrication of AlGaN/GaN multi-heterostructure and their application to UV/Blue light emitting devices", July 1992 MRS conference.
23. C. Eddy, Ph.D. Thesis, Boston University, Boston, MA, 1990.
24. T. Lei and T. D. Moustakas, *J. Appl. Phys.*, **71**, 4933 (1992).
25. Z. J.Yu, B. S. Sywe, A. U. Ahmed, J. H. Edger, *J. Electr. Mater.*, **21**, 782 (1992).
26. J. Sumakeris, Z. Sitar, K. S. Ailey-Trent, K. L. Moore and R. F. Davis, "Layer-by-Layer Epitaxial Growth of GaN at Low Temperatures," (to be published in Thin Solid Films).
27. *CRC Handbook of Metal Etchants*, eds. P.Walker and W. H. Tarn (CRC Press, Boca Raton, LA, 1991).
28. E. S. Dettmer, B. M. Romenesko, H. K. Charles Jr., B. G. Carkhuff and D. J. Merrill, *IEEE Transactions - Components, Hybrids, Manuf. Technol.*, **12**, 543 (1989).
29. L. B. Rowland, Ph.D. Thesis, North Carolina State University, Raleigh, NC, 1992.
30. D. Suryanarayana, *J. Am. Cer. Soc.*, **73**, 1108 (1990).
31. A. D. Katnani and K. I. Papathomas, *J. Vac. Sci. Technol.*, **A5**, 1335 (1987).
32. A. Abid, R. Bensalem and B. J. Sealy, *J. Mater. Sci.*, **21**, 1301 (1986).
33. T. Sato, K. Haryu, T. Endo and M. Shimado, *J. Mater. Sci.*, **22**, 2277 (1987).
34. D. Suryanarayana, L. J. Matienzo and D. F. Spencer, *IEEE Transactions - Components, Hybrids, Manuf. Technol.*, **12**, 566 (1989).
35. V.M. Donnelly and D.L. Flamm, *Solid State Technol.*, April 1981, p. 161.
36. G. S. Oehrlein, in *Handbook of Plasma Processing Technology*, eds. S. M. Rossnagel, J. J Cuomo and W. D. Westwood, (Noyes Publications, Park Ridge, New Jersey, 1990).

VIII. Distribution List

Mr. Max Yoder
Office of Naval Research
Electronics Program–Code 1114
800 North Quincy Street
Arlington, VA 22217

Office of Naval Research
Resident Representative
The Ohio State Univ. Research Center
1960 Kenny Road
Columbus, OH 43210-1063

Director
Naval Research Laboratory
Attention: Code 2627
Washington, DC 20314

Defense Technical Information Center
Building 5
Cameron Station
Alexandria, VA 22314

Robert J. Markunas
Research Triangle Institute
Post Office Box 12194
Research Triangle Park, NC 27709-2194

Howard Schmidt and Mark Hammond
Schmidt Instruments
2476 Bolsover, Suite 234
Houston, TX 77004

Professor R. F. Davis
Materials Science and Engineering
Box 7907
North Carolina State University
Raleigh, NC 27695-7907

Robert C. Linares
Linares Management Assoc., Inc.
P. O. Box 336
Sherborn, MA 01770

Maj. Gernot Pomrenke
AFOSR/NE
Bldg. 410
Bolling AFB, DC 20332

Dr. Andrew Freedman
Aerodyne Research, Inc.
45 Manning Road
Billerica, MA 01821

Duncan Brown
Advanced Technology Materials
7 Commerce Drive
Danbury, CT 06810

Walt Drozdoski
Booz-Allen
4330 East-West Highway
Bethesda, MD 20814-4455

Prof. Theodore D. Moustakas
Electrical Engineering
Boston University
44 Cummington Street
Boston, MA 02215

Prof. Jacques I. Pankove
Electrical & Computer Engineering
University of Colorado
Campus Box 425
Boulder, CO 80309-0425

Calvin Carter
Cree Research, Inc.
2810 Meridian Parkway
Durham, NC 27713

Prof. Benjamin Segall
Physics
Case Western Reserve Univ.
Cleveland, OH 44106

Dr. Walter Lambert
Physics
Case Western Reserve Univ.
Cleveland, OH 44106

Dr. William J. Schaff
Electrical Engineering
Cornell University
Ithaca, NY 14853

Barbara Goldenberg
Sensor & Systems Development Ctr.
10701 Lyndale Ave., S.
Honeywell, Inc.
Bloomington, MN 55420

Prof. Mike Spencer
Electrical Engineering
Howard University
Washington, DC 20059

Joshua Halpern
Department of Chemistry
Howard University
Washington, DC 20059

David Arch
Sensor & Systems Development Ctr.
10701 Lyndale Ave. S.
Honeywell, Inc.
Bloomington, MN 55420

J. Albert Schultz
Ionwerks
2215 Addison
Houston, TX 77030

Prof. Hadis Morkoc
1101 West Springfield Ave.
Urbana, IL 61801

Prof. Joe Greene
Dept. of M. S. E.
University of Illinois
1101 W. Springfield Ave.
Urbana, IL 61801

Dr. Dennis Wickenden
Johns Hopkins University
Applied Physics Laboratory
Johns Hopkins Road
Laurel, MD 20723

Jim Edgar
Dept. of Chem. Engr.
Room 105, Durland Hall
Kansas State Univ.
Manhattan, Kansas 66506-5102

Prof. Roy Clarke
Physics, Randall Hall
Univ. of Michigan
Ann Arbor, MI 48109

Prof. Philip L. Cohen
Dept. of Electrical Engineering
University of Minnesota
Minneapolis, MN 55455

Prof. Max Swanson
Prof. Nalin Parikh
Physics
University of North Carolina
Chapel Hill, NC 27590-3255

Prof. Manijeh Razeghi
Director, Center for Quantum Devices
Northwestern Univ.
2145 Sheridan Road
Evanston, IL 60208-3118

A. M. Goodman, ONR-1114
800 N. Quincy St.
Arlington, VA 22217-5660

J. Pazik, ONR-1113
800 N. Quincy St.
Arlington, VA 22217-5660

Prof. Walter Yarborough
271 Materials Research Lab
Penn State University
University Park, PA 16802

Prof. W. J. Choyke
Physics
University of Pittsburgh
Pittsburgh, PA 15260

Prof. Mark P. D'Evelyn
Chemistry
William March Rice University
P. O. Box 1892
Houston, TX 77251

H. Paul Maruska
Mgr. Photonics & Photovoltaics
Spire Corp.
1 Patriots Park
Bedford, MA 01730

P. Daniel Dapkus
University of Southern California
University Park
Los Angeles, CA 90089-1147

C. Buddie Mullins
Chemistry Engineering
University of Texas
Austin, TX 78712-1062

Prof. Michael Shur
Dept. of Electrical Engineering
University of Virginia
Charlottesville, VA 22903

Prof. Towe
E214 Thornton Hall
University of Virginia
Charlottesville, VA 22903